clinical bioenergetics

MDPI

Article

Sedentarism Exhibits a Distinct Mitochondrial Bioenergetic Phenotype Detectable by Cardiopulmonary Exercise and Lactate Testing (CPELT)

Inigo San-Millan [1,*], Janel L. Martinez [1], Genevieve C. Sparagna [2], Angelo D'Alessandro [3], Davide Stefanoni [3], Travis Nemkov [3] and John Hill [1]

[1] Division of Endocrinology, Metabolism and Diabetes, Department of Medicine, University of Colorado Anschutz Medical Campus, Aurora, CO 80045, USA
[2] Division of Cardiology, Department of Medicine, University of Colorado Anschutz Medical Campus, Aurora, CO 80045, USA
[3] Department of Biochemistry and Molecular Genetics, University of Colorado Anschutz Medical Campus, Aurora, CO 80045, USA
* Correspondence: inigo.sanmillan@cuanschutz.edu

Abstract

Background: Physical inactivity is a major contributor to cardiometabolic disease and mortality. Although mitochondrial dysfunction characterizes overt pathology, whether sedentarism constitutes a distinct and measurable bioenergetic disease state, rather than simply reduced fitness, has not been established. **Methods:** Nine sedentary (SED) and ten physically active (AC) healthy males (42 ± 14 yr) were studied. Skeletal muscle bioenergetics were assessed using high-resolution respirometry, fluxomics, metabolomics, and protein expression analyses. Whole-body physiology was evaluated using cardiopulmonary exercise and lactate testing (CPELT). **Results:** At rest, SED exhibited marked reductions in mitochondrial capacity, including Complex I (−36%), Complex II (−28%), electron transport system capacity (−34%), and ATP-synthase-coupled respiration (−30%, all $p < 0.01$). The most pronounced alteration was a 49% reduction in mitochondrial pyruvate carrier (MPC1) expression, which closely correlated with reduced pyruvate oxidation (−37%, $p = 0.006$) and lower TCA intermediates. SED also showed reduced MCT1 abundance, impaired fatty-acid oxidation capacity (−32% to −35%), decreased CPT1 activity (−51%), altered cardiolipin composition, and elevated ROS/O_2 flux ratios. During exercise, SED demonstrated lower VO_2max (−38%), reduced fat oxidation (−35%), and higher blood lactate accumulation (>60%, $p < 0.001$). Mitochondrial function was strongly associated with exercise performance (r = 0.57–0.78, $p < 0.01$). **Conclusions:** Healthy sedentary adults displayed a coordinated reduction in tissue-level mitochondrial oxidative capacity, substrate-handling markers, cardiolipin abundance, and metabolic flexibility. These findings should be interpreted as an integrated per-mg skeletal-muscle bioenergetic phenotype in which lower mitochondrial density may account for much of the observed reduction. Within this phenotype, the 49% reduction in MPC1 alongside preserved GLUT4, LDHA, and LDHB abundance represents an outstanding differential observation that future studies with direct mitochondrial-content normalization should test. CPELT-derived fat oxidation and blood lactate responses reflected this tissue-level bioenergetic phenotype, providing candidate noninvasive physiological markers for future longitudinal and interventional studies.

Keywords: mitochondrial function; MPC1; pyruvate oxidation; sedentary lifestyle; cardiolipin; ROS; metabolic flexibility; CPELT

Academic Editor: Olga Golubnitschaja

Received: 30 March 2026
Revised: 12 June 2026
Accepted: 18 June 2026
Published: 25 June 2026

1. Introduction

Physical inactivity is a global health crisis, contributing to over 5 million deaths annually through non-communicable diseases (NCDs) such as cardiovascular disease (CVD), type 2 diabetes (T2D), Alzheimer's disease (AD), Parkinson's disease, depression, dementia, and cancer [1–14]. Low cardiorespiratory fitness (CRF) is the leading attributable risk factor for all-cause mortality, surpassing smoking and obesity [15]. The World Health Organization (WHO) reports that 27.5% of adults and 81% of adolescents fail to meet physical activity guidelines, projecting 500 million new NCD cases by 2030, with treatment costs of ~US$27 billion annually and billions more in productivity losses [16].

Physical activity is a canonical characteristic of humans. Nevertheless, in modern societies, the normalization of the lack of physical activity has led to the perception that physical activity is an intervention even though it remains as the *modus vivendi* engrained in our genes. The reality is that becoming sedentary has been the real intervention and collateral effect of modern societies [17]. This evolutionary perspective challenges the use of "healthy sedentary" individuals as controls in medical research. The concept of the "healthy sedentary" individual is therefore biologically inconsistent and may instead represent an early stage of bioenergetic dysfunction rather than a true physiological control state. Skeletal muscle is responsible for ~80–85% of glucose disposal under resting and hyperinsulinemic–euglycemic postprandial conditions [18], and therefore it is a critical site for studying cellular metabolism, mitochondrial function, and bioenergetics. Mitochondrial dysfunction is implicated in the pathogenesis of NCDs, including T2D, CVD, AD, and even cancer, all characterized by impaired oxidative phosphorylation (OXPHOS) and substrate metabolism [17]. Once glucose enters the cell through GLUT transporters, glycolysis converts it to pyruvate, which, under normal flux and resting conditions, should enter mitochondrial for complete oxidation through OXPHOS in the electron transport chain (ETC). The discovery of the mitochondrial pyruvate carrier (MPC) in 2012 [19,20] revolutionized our understanding of glucose metabolism, highlighting pyruvate transport as a pivotal step linking glycolysis to mitochondrial ATP production. Dysregulated MPC may precede insulin resistance, offering a novel therapeutic target.

Despite the global burden of sedentarism, few studies have characterized the metabolic and bioenergetic profiles of "healthy sedentary" individuals compared to moderately active counterparts, the true evolutionary control. Early studies focused on overt disease states (e.g., T2D and obesity), but subclinical impairments in sedentary individuals could provide a preventive window. Mitochondrial respiration, substrate oxidation (carbohydrates, fatty acids, and amino acids), MPC content, reactive oxygen species (ROS), and lipid composition (e.g., cardiolipin) are key indicators of cellular health. Additionally, exercise-based assessments like CPELT can reveal metabolic flexibility and lactate clearance, potentially mirroring resting mitochondrial function noninvasively [21], which offers significant possibilities for earlier diagnosis, prevention through exercise and nutrition, as well as even the development of novel therapeutics.

Herein, we aimed to characterize mitochondrial and bioenergetic signatures in sedentary (SED) vs. moderately active (AC) individuals, using resting muscle biopsies (high-resolution respirometry, fluxomics, metabolomics, protein expression, and cardiolipin analysis) and exercise testing (CPELT, fat/carbohydrate oxidation, and lactate clearance).

Contemporary integrative frameworks of skeletal muscle metabolism recognize that substrate selection and glucose handling depend on multiple interacting determinants, including insulin signaling and GLUT4 translocation, mitochondrial content, fractional mitochondrial utilization at a given work rate, oxidative enzyme activity, and lipid handling [22–25]. Within this framework, lower mitochondrial content per unit muscle is itself sufficient to shift fuel selection toward carbohydrate, raise the relative respiratory

load on each mitochondrion at any given VO_2, and promote earlier glycolytic reliance and lactate accumulation. Building on this established framework, we asked whether substrate-entry steps internal to the mitochondrion, in particular, pyruvate transport via MPC1 and long-chain fatty-acid transport via CPT1, are also altered in healthy sedentary muscle. In adults with normal GLUT4 expression, we observed coordinated reductions in mitochondrial respiratory capacity together with a selective decrease in MPC1 abundance and pyruvate-stimulated respiration. We interpret these findings as complementing, rather than displacing, existing integrative models by drawing attention to mitochondrial substrate-entry as an additional and potentially diagnostically tractable locus of impairment in sedentary skeletal muscle.

We hypothesized that SED individuals exhibit significant mitochondrial impairments, detectable at rest and during exercise, which could be assessed noninvasively via CPELT. Our findings reveal early bioenergetic decline in SED, offering insights into NCD prevention and novel therapeutic targets like MPC.

2. Materials and Methods

2.1. Subject Recruitment

Nineteen healthy male subjects (age: 41.9 ± 13.8 years) were recruited and assigned to two groups according to their habitual physical activity levels. Sedentary (SED, n = 9): No regular exercise or elevated heart rate beyond daily tasks. Active (AC, n = 10): ≥150 min/week aerobic exercise for ≥6 months. Anthropometric characteristics were as follows: the sedentary group (n = 9) exhibited a mean body weight of 90.1 ± 23.7 kg, height of 177.6 ± 5.7 cm, and body mass index (BMI) of 28.3 ± 6.0 $kg{\cdot}m^{-2}$. The active group (n = 10) presented a mean body weight of 78.5 ± 6.0 kg, height of 181.6 ± 4.0 cm, and BMI of 23.8 ± 1.0 $kg{\cdot}m^{-2}$.

Exclusion criteria: Diagnosed diabetes (type 1 or 2), or cardiovascular risk per American College of Sports Medicine (ACSM) Risk Stratification Model. All subjects provided informed consent. The study was approved by the Colorado Multiple Institutional Review Board (protocol code 17-1095; approval date, 6 November 2018).

2.2. Pre-Test Standardization

To minimizes the influence of acute dietary intake and prior physical activity on resting substrate partitioning, mitochondrial respiration, and circulating metabolites, all participants followed a standardized pre-test protocol. Participants refrained from any structured or vigorous physical activity for at least 48 h prior to both the muscle biopsy and the cardiopulmonary exercise and lactate testing (CPELT) session. On the day preceding each testing visit, participants consumed their habitual mixed diet and were instructed to avoid alcohol, caffeine, and exceptionally large meals. Both the resting muscle biopsy and the CPELT session were performed in the morning following an overnight fast of at least 10 h (water ad libitum). For the CPELT session, in addition to the overnight fast, participants were instructed to consume >50% of total energy as carbohydrates during the day preceding the test (verified via 24 h food logs reviewed on arrival), as previously described [21]. Adherence to fasting, abstention from exercise, and dietary instructions was confirmed verbally on arrival at each visit.

2.3. Muscle Biopsies

Biopsies (~75 mg total) from the vastus lateralis were obtained under ultrasound guidance using a Bard Monopty Disposable Core Biopsy Instrument (BD, Franklin Lakes, NJ, USA) (12 gauge × 10 cm) after local anesthesia (5 mL 1% lidocaine HCl; Pfizer, New York, NY, USA) and Ethyl Chloride spray (Gebauer Company, Cleveland, OH, USA)).

Three passes yielded ~25 mg tissue each. Samples were immediately processed fresh for respirometry or flash-frozen in liquid nitrogen and stored at −80 °C. Incisions were closed with Steri-strips (3M, St. Paul, MN, USA)) and Elastoplast tape. n = 10/group.

2.4. High-Resolution Respirometry and ROS Production

Permeabilized muscle fibers (~10 mg) were prepared in BIOPS (10 mM Ca-EGTA, 0.1 µM free calcium, 20 mM imidazole, 20 mM taurine, 50 mM K-MES, 0.5 mM DTT, 6.56 mM $MgCl_2$, 5.77 mM ATP, and 15 mM phosphocreatine, pH 7.1) with 30 µg/mL saponin for 30 min. Fibers were washed for 10 min at 4 °C in ice-cold mitochondrial respiration medium [26]. Samples were blotted on filter paper, weighed, and placed in the chambers of the Oroboros O2K apparatus (Oroboros Instruments, Innsbruck, Austria) at 37 °C containing respiration medium. Substrates were added sequentially: palmitoylcarnitine (0.2 mM) + malate (1 mM) + ADP (4 mM) for long-chain fatty-acid oxidation; octanoylcarnitine (0.4 mM) for medium-chain; pyruvate (5 mM) for Complex I via pyruvate dehydrogenase; glutamate (10 mM) for Complex I independent of PDH; succinate (10 mM) for Complex II; FCCP (1 µM) for maximal ETS capacity; rotenone (2 µM) for Complex II; and antimycin A (5 µM) for residual oxygen consumption (ROX). ROS was measured via Amplex Red (Thermo Fisher Scientific, Waltham, MA, USA) (5 units/mL SOD, 1 unit/mL horseradish peroxidase, 0.1 µM/step H_2O_2 calibration). O_2 flux normalized to tissue wet weight. n = 10/group. Figure 1 summarizes the muscle biopsy procedure followed by mitochondrial respirometry.

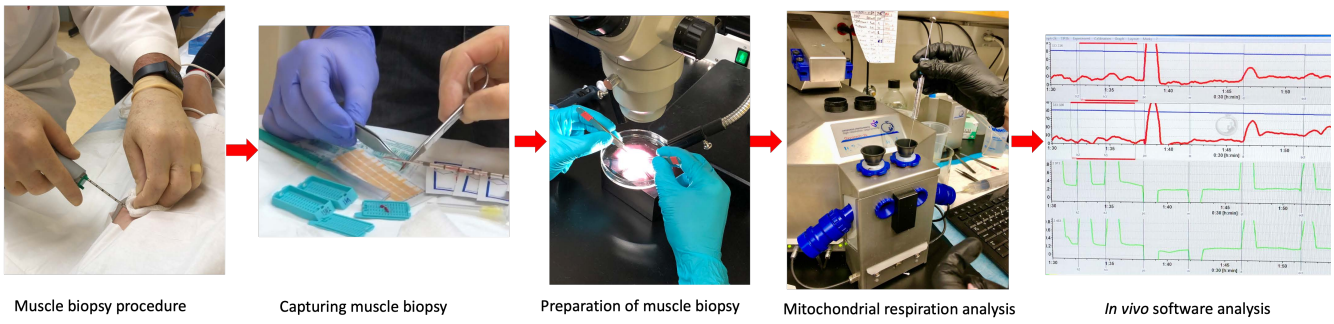

Figure 1. Muscle biopsy procedure included extraction, mitochondrial homogenization, and mitochondrial respiration analysis through Oroboros O2K.

2.5. Protein Expression

Skeletal-muscle homogenates were analyzed via capillary-based Western (JESS, ProteinSimple, San Jose, CA, USA). Antibodies: GLUT4 (Abcam, ab654, Cambridge, UK, 1:1000), LDHA (Cell Signaling Technology, Danvers, MA, USA #2012, 1:500), LDHB (Cell Signaling #8176, 1:500), and MPC1 (Abcam ab176559, 1:800). Samples were denatured (95 °C, 5 min) with fluorescent master mix (1:4). Protein peak areas were normalized to total protein using the Compass for Simple Western software (version 6.1.0) (ProteinSimple, San Jose, CA, USA). Antibody specificity was validated via molecular weight controls; n = 9–10/group (minor sample loss in 1 SED). A representative Jess capillary electropherogram for MPC1 (~12 kDa) with the vinculin loading control (~116 kDa) across the full cohort is provided as Supplementary Figure S1.

2.6. Carnitine Palmitoyltransferase I and II Activity

CPT1 and CPT2 activity was quantified in muscle homogenates using a ^{14}C-carnitine radioassay [21]. CPT1: Plasma membrane was permeabilized, measuring palmitoylcarnitine production from palmitoyl-CoA. CPT2: Mitochondrial inner membrane was permeabilized with malonyl-CoA to inhibit CPT1. n = 9–10/group.

2.7. Skeletal Muscle Isotope Tracing

Fresh tissue (~10 mg) was incubated (37 °C, 30 min) in Krebs-Ringer bicarbonate solution with 2 mM $^{13}C_3$-pyruvate (CLM-2440-PK, Cambridge Isotope Laboratories, Tewksbury, MA, USA) or 2 mM $^{13}C_1$-lactate (CLM-1577-PK, Cambridge Isotope Laboratories, Tewksbury, MA, USA). Samples were centrifuged at 2000× *g* for 10 min, flash-frozen, and stored at −80 °C. n = 9–10/group.

2.8. Mass Spectrometry-Based Metabolomics

Muscle tissue was extracted in methanol:acetonitrile:water (5:3:2) at 30 mg/mL, vortexed (4 °C, 30 min), and centrifuged at 10,000× *g*, 10 min at 4 °C). Supernatants were analyzed via UHPLC-MS (Vanquish UHPLC and Q Exactive mass spectrometer, Thermo Fisher Scientific, Waltham, MA, USA) over a Kinetex C18 column (2.1 × 150 mm, 1.7 µm; Phenomenex, Torrance, CA, USA). Mobile phases: Positive ion (water + 0.1% formic acid; acetonitrile + 0.1% formic acid); negative ion (water:acetonitrile 95:5 + 1 mM ammonium acetate; acetonitrile:water 95:5 + 1 mM ammonium acetate). Gradient: 5% to 95% B over 1 min, hold at 95% B for 2 min (400 µL/min, 45 °C). Full MS mode (60–900 *m*/*z*, 70,000 resolution). Data converted to mzXML (MS Convert, ProteoWizard, Palo Alto, CA, USA), processed in El-MAVEN (version 0.12.0, Elucidata, Cambridge, MA, USA) for metabolite assignments and isotopologue distributions, and corrected for natural isotope abundances. Median-normalized, range-scaled data analyzed via MetaboAnalyst (version 6.0, www.metaboanalyst.ca, McGill University, Montreal, QC, Canada) (PLS-DA, hierarchical clustering). n = 10/group (292 metabolites quantified). Figure 2 summarizes the procedure.

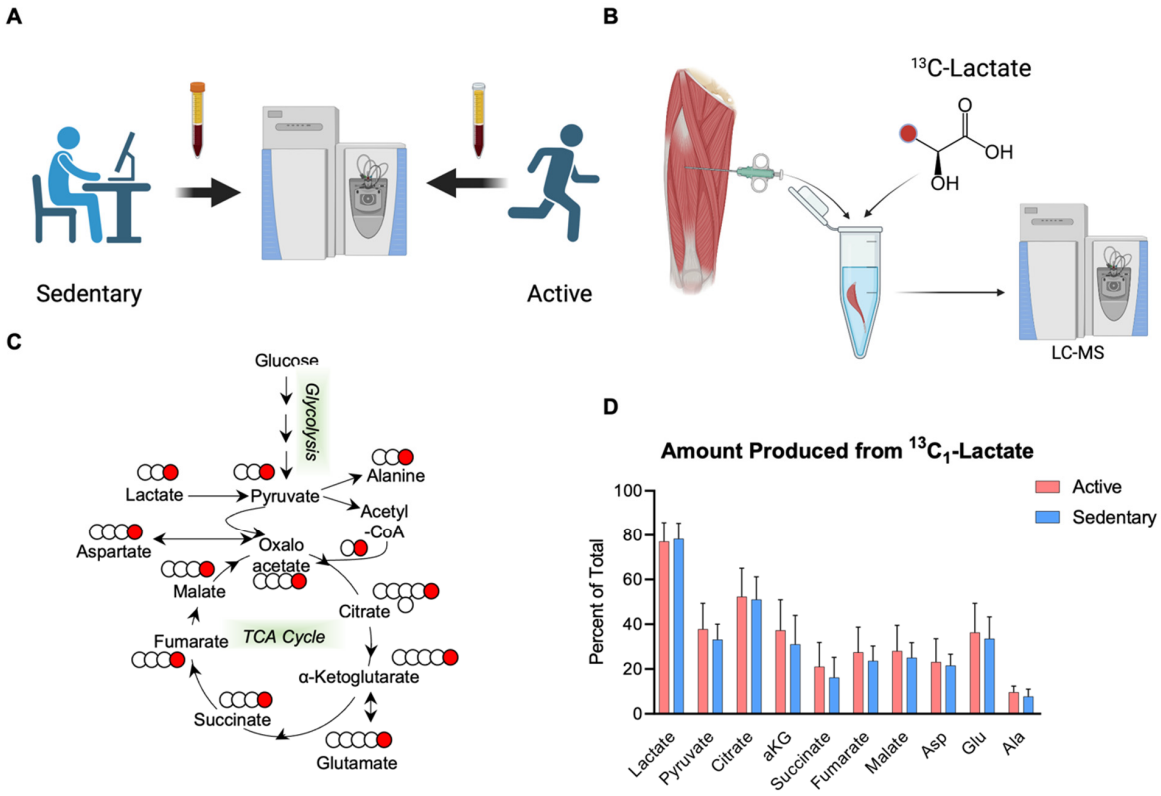

Figure 2. Ex vivo skeletal muscle isotope-tracing analysis. (**A**) Skeletal muscle was isolated from 10 sedentary and 13 active individuals. (**B**) Isolated tissue was incubated with $^{13}C_1$-lactate for 30 min in a physiological buffer at 37 °C. (**C**) Isotope tracing was targeted to metabolites in the TCA cycle and related transaminase products. (**D**) Isotope enrichment is reported as a percentage of the total pool in each sample.

2.9. Cardiolipin Quantification

Lipid extracts from homogenized muscle (PBS) were analyzed via LC/MS (API 4000 (Sciex, Framingham, MA, USA)) using normal phase solvents [27]. Total cardiolipin (CL) was the sum of seven dominant species (m/z 1422, 1446, 1448, 1450, 1470, 1472, and 1474). L4CL percentage was calculated. n = 9–10/group.

2.10. Graded Exercise Assessment

Subjects consumed >50% kcal as carbohydrates the night before/day of testing (verified via food logs). Exercise was performed on a cycle ergometer (KICKR Smart Trainer, Wahoo Fitness, Atlanta, GA, USA). Warm-up: <65 W for 10 min. Protocol: Start at 75 W, and increase by 25 W every 10 min until volitional exhaustion (inability to maintain 60 rpm). All subjects reached $\geq$150 W. n = 9–10/group.

2.11. Gas Exchange Measurements

VO_2, VCO_2, and respiratory exchange ratio (RER = VCO_2/VO_2) were measured via ParvoMedics TrueOne 2400 (Sandy, UT, USA), averaged over 15 s intervals. n = 9–10/group.

2.12. Fat and Carbohydrate Oxidation Rates

Calculated per Frayn [28]:

- FATox ($g \cdot min^{-1}$) = 1.695 $\times$ VO_2($L \cdot min^{-1}$) $-$ 1.701 $\times$ VCO_2($L \cdot min^{-1}$);
- CHOox ($g \cdot min^{-1}$) = 4.585 $\times$ VCO_2($L \cdot min^{-1}$) $-$ 3.226 $\times$ VO_2($L \cdot min^{-1}$); n = 10/group.

2.13. Lactate Concentration Measurement

Capillary blood from the earlobe was analyzed for L-lactate (Lactate Plus Meter, Nova Biomedical, Waltham, MA, USA) at each stage's end. Heart rate (Polar S725x (Polar Electro, Kempele, Finland)) and perceived exertion were monitored. n = 9–10/group.

2.14. Statistical Analysis

Data were analyzed in GraphPad Prism (version 9.2.1, GraphPad Software, San Diego, CA, USA). Independent t-tests were performed with the Shapiro–Wilk normality test; Cohen's d was used for effect sizes. Bonferroni correction was used for multiple comparisons (α = 0.05/num tests). Pearson correlations were used for rest–exercise relationships; Spearman's was used if non-normal. Data: Mean $\pm$ SD; $p < 0.05$ significant, $p < 0.1$ as trending. Power analysis (80% power, α = 0.05) estimated n = 9–10/group sufficient for large effects (d > 1.0).

3. Results

3.1. Mitochondrial Respiration and Oxidative Capacity

At rest, sedentary individuals (SED) exhibited marked deficits across multiple components of the mitochondrial electron transport system (ETS) when compared with active individuals (AC) (Figure 3A–D). Oxygen flux through Complex I, supported by pyruvate, glutamate, and malate, was 36% lower in SED (p = 0.008, d = 1.8), and Complex II-supported respiration, indexed by the increment following succinate addition, was 28% lower (p = 0.042, d = 1.2), indicating attenuated NADH- and $FADH_2$-driven electron flow through the respiratory chain. The deficit extended to total ETS capacity, which was 34% lower in SED (p = 0.007, d = 1.7) and to ETS coupled to ATP synthase (P_ATP), which was reduced by 30% (p = 0.009, d = 1.5). Together, these data demonstrate a generalized reduction of maximal mitochondrial respiratory capacity in sedentary skeletal muscle.

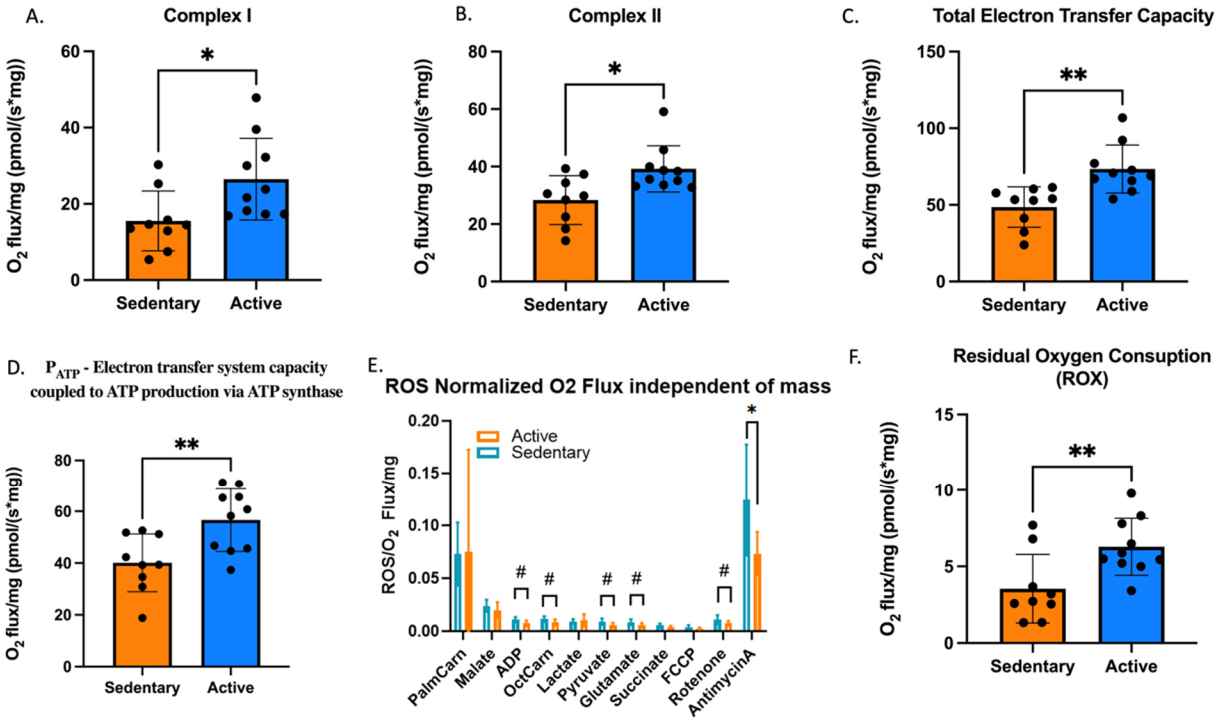

Figure 3. Differences in (**A**) Complex I respiration (pyruvate + glutamate + malate, ADP-stimulated state). (**B**) Complex II respiration after succinate addition. (**C**) Total electron transfer system (ETS) capacity after FCCP titration (maximal uncoupled respiration). (**D**) ATP-synthase-coupled (OXPHOS) respiration in the ADP-replete state. (**E**) Differences in reactive oxygen species (ROS) production normalized to O_2 flux independent of mass in sedentary and active individuals. (**F**) Differences in residual oxygen consumption (ROX) due to oxidative side reactions that continue after the inhibition of the ET pathway. # trend toward significance; * $p < 0.05$; ** $p < 0.01$.

3.2. Reactive Oxygen Species Production

Reactive oxygen species (ROS) production, when normalized to O_2 flux, revealed further distinctions between groups (Figure 3E,F). While absolute ROS emission tended to be higher in AC, normalization to O_2 flux indicated greater oxidative stress burden in SED, particularly following antimycin A inhibition ($p = 0.048$, d = 1.1), with similar upward trends observed during ADP-, octanoylcarnitine-, pyruvate-, and glutamate-driven respiration stages ($p < 0.10$). These findings point to a lower redox efficiency in sedentary muscle, where a greater fraction of electrons is diverted toward ROS generation rather than productive respiration.

By contrast, active individuals produced higher absolute ROS, consistent with their greater respiratory flux. When normalized to O_2 flux, active individuals showed a lower net ROS/O_2 ratio, a pattern that may reflect either greater mitochondrial respiratory efficiency or superior intra-mitochondrial antioxidant buffering capacity in trained muscle; however, the present data cannot distinguish between these interpretations.

Furthermore, residual oxygen consumption (ROX), the non-phosphorylating respiration that persists after inhibition with antimycin A, was significantly higher in active individuals ($p = 0.007$, d = 1.4) (Figure 3F). ROX reflects oxygen use not linked to ATP synthesis, associated with baseline mitochondrial maintenance and proton leak. The higher ROX observed in active muscle suggests greater mitochondrial density and metabolic turnover, indicative of a more dynamic and resilient oxidative system.

3.3. Protein Expression and Enzyme Activity

Skeletal-muscle expression of GLUT4, LDHA, and LDHB was similar between active (AC) and sedentary (SED) individuals (Figure 4A,C,D), indicating comparable basal capacity for glucose uptake and cytosolic lactate interconversion. Despite similar GLUT4 content, MPC1 expression (the mitochondrial pyruvate carrier subunit critical for pyruvate transport into the matrix) was markedly lower in SED, reduced by 49% relative to AC ($p = 0.005$, d = 2.1). This deficit strongly correlated with diminished pyruvate-driven respiration, suggesting a functional limitation in the entry of glycolytic carbon into oxidative pathways.

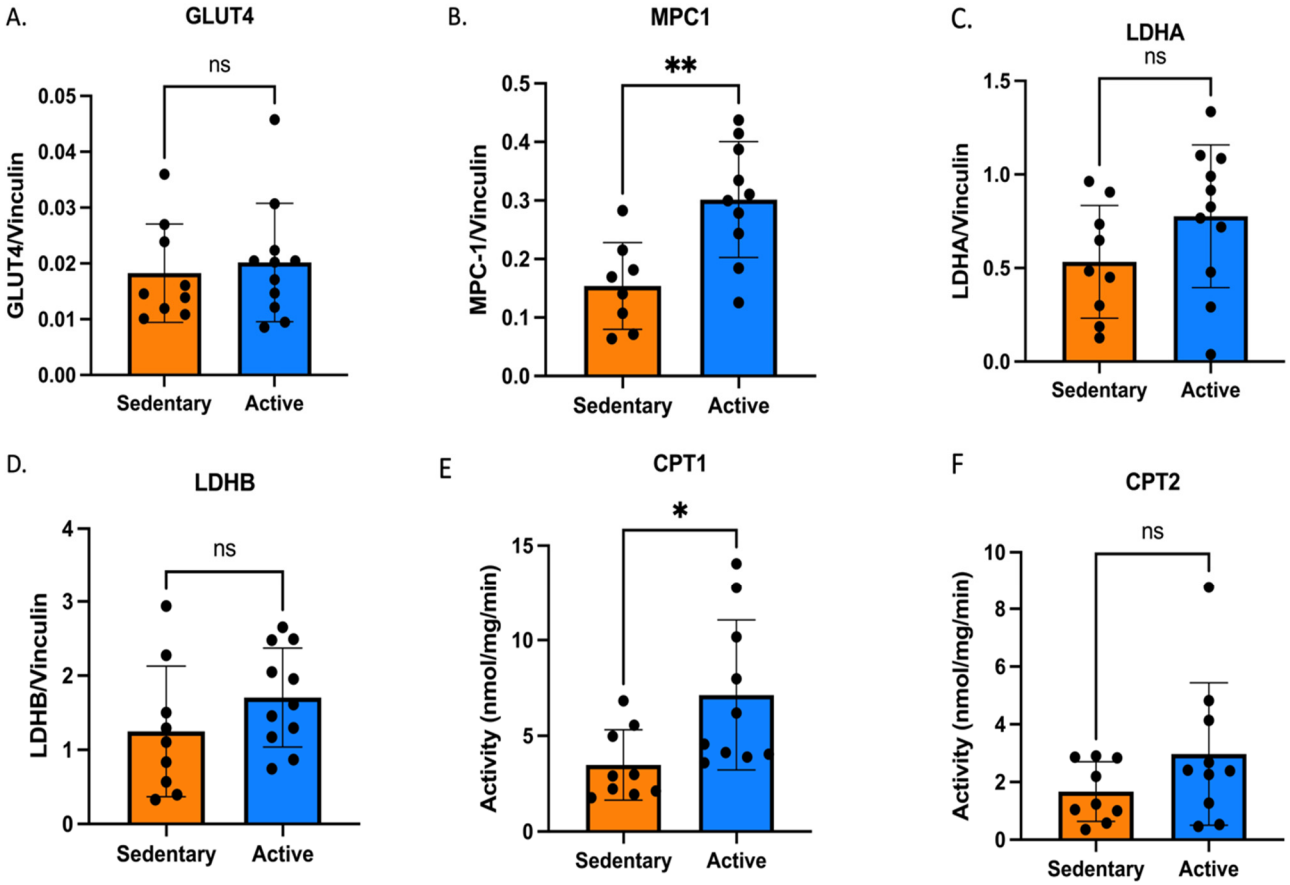

Figure 4. Differences in protein expression between SED and ACT individuals of (**A**) GLUT4, (**B**) MPC1, (**C**) LDHA, (**D**) LDHB, (**E**) CPT1, and (**F**) CPT2 between sedentary and active individuals. ns = non-statistical significance; * $p < 0.05$; ** $p < 0.01$.

In parallel, CPT1 activity, the rate-limiting enzyme for long-chain fatty-acid transport across the outer mitochondrial membrane, was 51% lower in SED ($p = 0.038$, d = 1.4), whereas CPT2 activity showed a downward trend without reaching significance ($p = 0.16$) (Figure 4E,F). Together, these findings indicate that sedentary muscle exhibits coordinated reductions in both pyruvate and fatty acid-handling capacity per unit tissue, consistent with a reduced ability to flexibly utilize carbohydrate and lipid substrates for mitochondrial oxidation and contributing to the diminished metabolic flexibility observed during CPELT.

3.4. Cardiolipin Composition

Mitochondrial phospholipid analysis revealed clear group differences in cardiolipin content and remodeling profiles (Figure 5A–E). Total cardiolipin and its dominant molecular species, tetralinoleoyl cardiolipin (L4CL), were significantly lower in sedentary individuals ($p = 0.007$ and $p = 0.006$, respectively; d ≈ 1.5–1.6). In contrast, the proportion of monolysocardiolipin (MLCL), a remodeling intermediate, was modestly higher in active

individuals (p = 0.049), resulting in a slightly elevated MLCL:CL ratio. These compositional differences suggest that active muscle maintains greater cardiolipin abundance and enrichment in the mature L4CL species, which is essential for optimal organization of respiratory supercomplexes and efficient electron transfer. Conversely, the lower total and tetralinoleoyl cardiolipin content observed in sedentary muscle is consistent with reduced inner-membrane phospholipid support for OXPHOS organization, in line with the observed declines in ETS capacity and ATP-linked respiration.

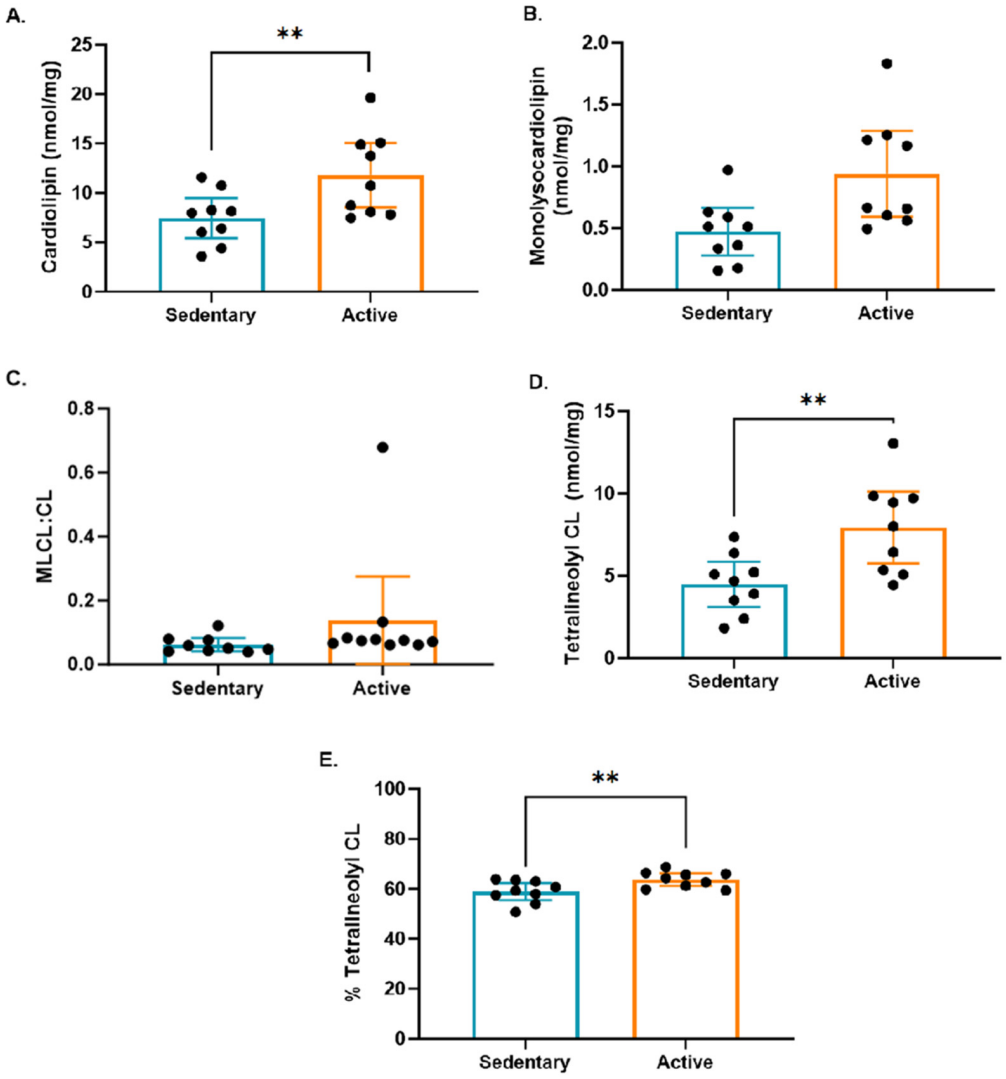

Figure 5. Cardiolipin content and molecular composition in skeletal muscle. (**A**) Total cardiolipin, (**B**) monolysocardiolipin, (**C**) MLCL:CL ratio, (**D**) tetralinoleoyl cardiolipin (L4CL), and (**E**) percent L4CL. Both total cardiolipin and L4CL were significantly higher in active individuals ($p < 0.01$), whereas MLCL showed a modest increase. Bars represent mean ± SD. ** $p < 0.01$.

3.5. Substrate-Specific Mitochondrial Oxidation

Substrate-dependent respiration revealed a consistent deficit across multiple oxidative pathways in sedentary individuals (Figure 6A–D). Pyruvate-supported O_2 flux was 37% lower in SED compared with active individuals (p = 0.006, d = 1.9), indicating reduced capacity for mitochondrial oxidation of glycolytic carbon. This finding aligns with the markedly lower MPC1 expression observed in SED muscle and is further corroborated by the reduced [^{13}C]-lactate labeling of TCA intermediates (Section 3.6), together indicating constrained mitochondrial pyruvate utilization in sedentary muscle.

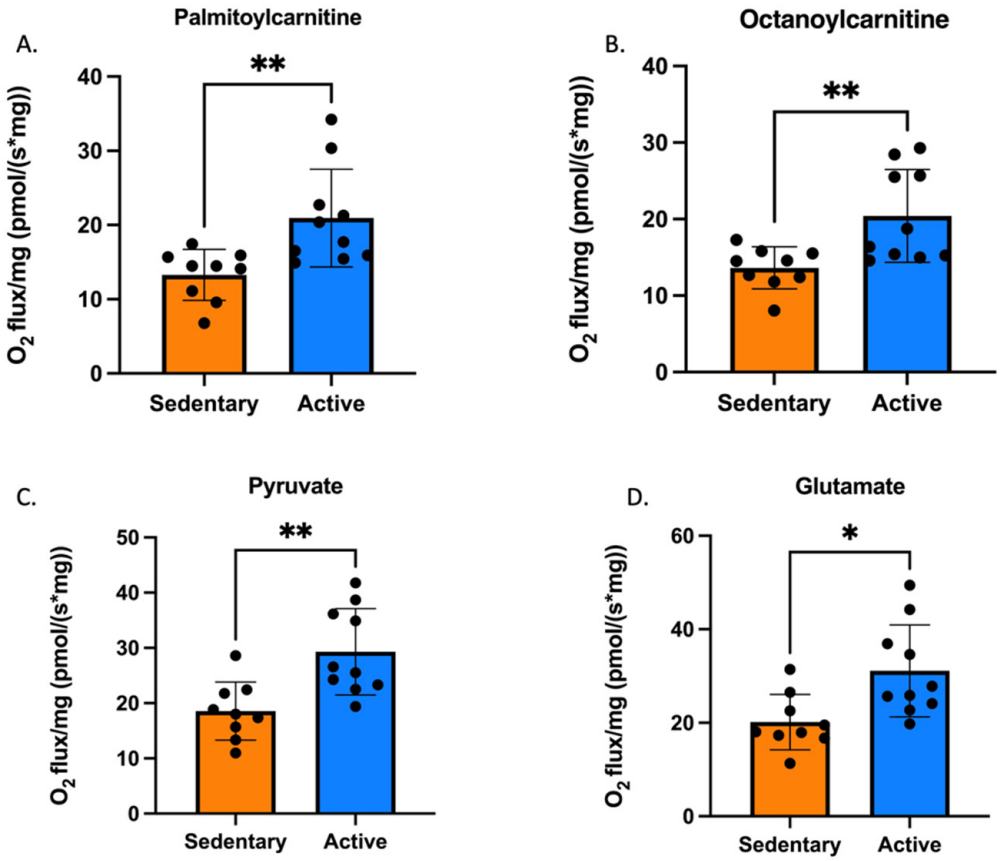

Figure 6. Differences in O_2 flux between sedentary and active individuals following sequential additions of (**A**) palmitoylcarnitine + malate + ADP (long-chain fatty-acid oxidation), (**B**) octanoylcarnitine (medium-chain fatty-acid oxidation), (**C**) pyruvate (Complex I via pyruvate dehydrogenase and MPC-mediated transport), and (**D**) glutamate (Complex I, PDH-independent). * $p < 0.05$; ** $p < 0.01$.

Similarly, long-chain fatty-acid oxidation using palmitoylcarnitine and medium-chain oxidation with octanoylcarnitine were lower in SED by 35% and 32%, respectively (both $p = 0.008$, d $\geq$ 1.5). These findings point to a parallel deficit in lipid-derived electron flux, consistent with the reduced CPT1 activity reported earlier. Glutamate-driven Complex I respiration was also reduced by 36% ($p = 0.008$, d = 1.5), reinforcing the notion of a global decline in oxidative substrate utilization.

Collectively, these results reveal that sedentary skeletal muscle exhibits a multifaceted reduction in substrate oxidation capacity, encompassing both carbohydrate- and lipid-derived pathways. The concurrent reductions in MPC1 expression and pyruvate oxidation capacity are consistent with reduced mitochondrial handling of glycolytic carbon, contributing to the diminished metabolic flexibility characteristic of the sedentary phenotype.

3.6. Metabolomic Profiling and [$^{13}C_1$]-Lactate Tracing

Multivariate analysis of the untargeted metabolomic data using PLS-DA (Figure 7A) demonstrated clear discrimination between sedentary (SED) and active (AC) individuals, with distinct group clustering and minimal overlap, indicating a robust separation based on metabolic phenotype. The volcano plot (Figure 7B) and heatmap (Figure 7C) further highlighted differential abundance patterns between groups.

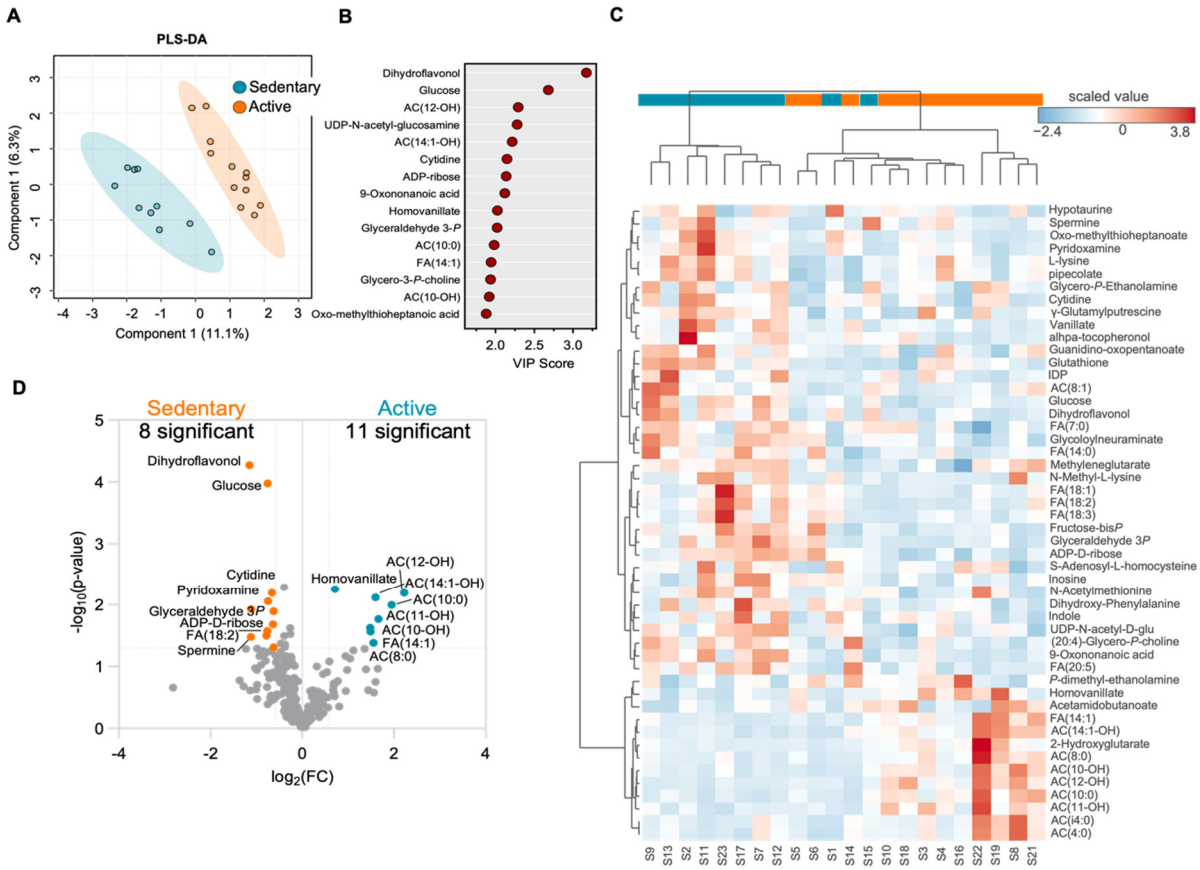

Figure 7. Untargeted metabolomics and [$^{13}C_1$]-lactate tracing in skeletal muscle. (**A**) PLS-DA plot showing distinct separation between sedentary and active individuals. (**B**) Volcano plot and (**C**) heatmap illustrating differential metabolite abundance, with higher glycolytic intermediates in sedentary muscle and elevated acylcarnitines and TCA metabolites in active muscle. (**D**) [$^{13}C_1$]-lactate tracing demonstrates reduced labeling of citrate and malate in sedentary individuals (−40% and −35%, $p < 0.01$), indicating lower incorporation of lactate-derived carbon into TCA-cycle intermediates.

SED muscle displayed central metabolic accumulation of glycolytic and upstream carbohydrate intermediates, including glucose-6-phosphate, fructose-1,6-bisphosphate, 3-phosphoglycerate, and phosphoenolpyruvate, along with elevated lactate and pyruvate, consistent with enhanced cytosolic glycolytic flux and reduced oxidative disposal. In contrast, AC muscle exhibited higher levels of short- and medium-chain acylcarnitines (C6–C12 species), succinate, and fumarate, reflecting greater lipid mobilization and mitochondrial TCA activity.

Stable-isotope tracing with [$^{13}C_1$]-lactate (Figure 7D) revealed markedly lower labeling of citrate (−40%) and malate (−35%) in SED muscle (both $p < 0.01$), indicating lower incorporation of lactate-derived carbon into TCA-cycle intermediates. This pattern closely parallels the lower MPC1 abundance and diminished pyruvate-supported respiration described earlier, and is consistent with reduced mitochondrial utilization of lactate-derived carbon in sedentary muscle.

Overall, these findings define a metabolic signature of inactivity characterized by glycolytic metabolite accumulation and constrained pyruvate–TCA coupling, contrasting with the broader substrate oxidation and acylcarnitine enrichment observed in active skeletal muscle.

3.7. Exercise Performance

The exercise results revealed further significant differences between AC and SED. AC displayed higher aerobic fitness and oxidation flexibility. Absolute and relative VO_2max were 31% and 38% greater, respectively (both $p < 0.0001$, d > 2.2) (Figure 8A,B). Maximal and relative absolute power output were 35% and 42% higher, respectively (both $p < 0.0001$) (Figure 8C,D). Blood lactate during moderate stages at 125 W and 150 W was higher in SED ($p < 0.001$, d ≈ 1.5) (Figure 8E,F).

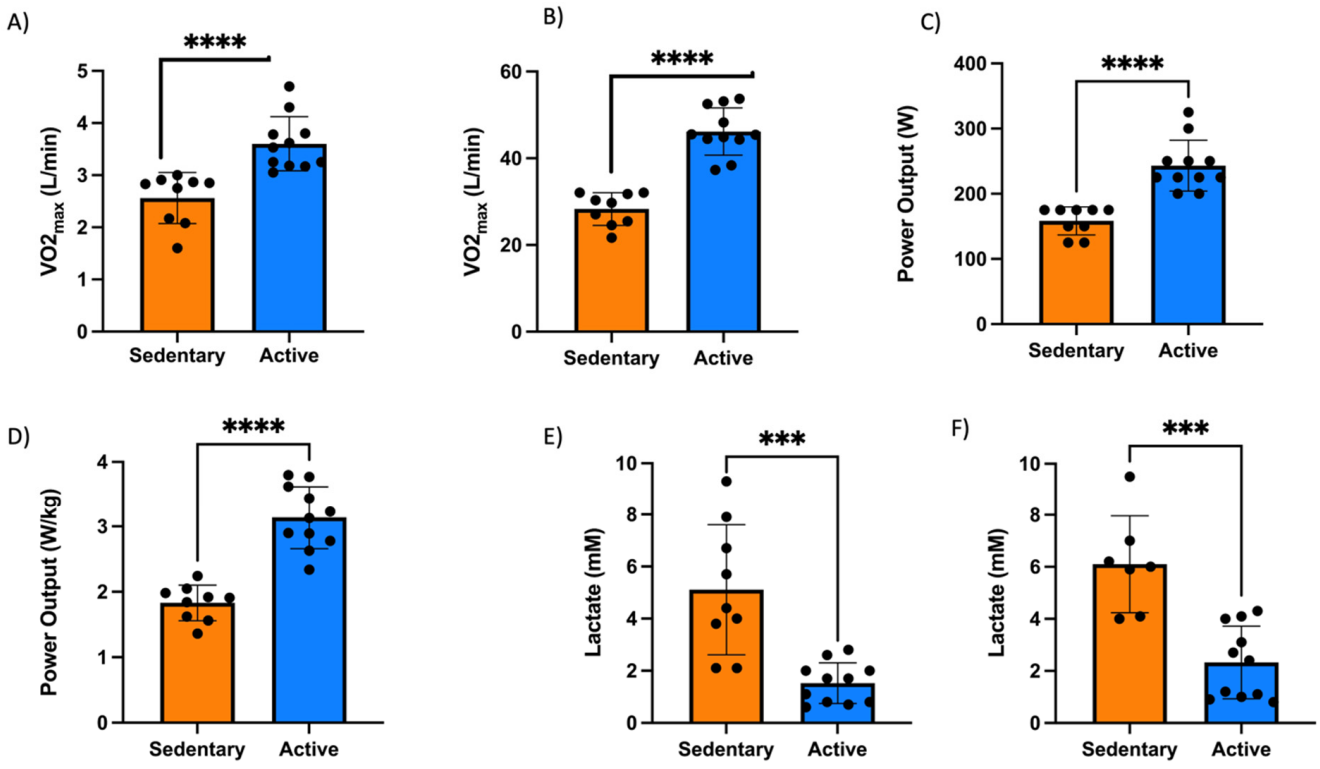

Figure 8. VO_2max, power output, and blood lactate differences between active (AC) and sedentary (SED) individuals. (**A**,**B**) VO_2max (absolute and relative). (**C**,**D**) Maximal and relative absolute power output. (**E**,**F**) Blood lactate concentrations at moderate exercise stages (125 W and 150 W). Black dots represent individual data points. *** $p < 0.001$; **** $p < 0.0001$.

3.8. Substrate Oxidation and Lactate Responses During Incremental Exercise

Figure 9A–F illustrate the distinct metabolic responses between active and sedentary individuals across increasing power outputs. In active individuals (Figure 9A,C,E), fat oxidation (FATox) progressively rises at low-to-moderate workloads and peaks before declining at higher intensities as carbohydrate oxidation (CHOox) and blood lactate concentrations increase. FATox reaches ~0.35–0.4 g·min^{-1} at ~150 W, with lactate remaining below 1 mM throughout this range (r = −0.99, $p < 0.001$), reflecting a high capacity for mitochondrial substrate oxidation and efficient redox balance. As workload increases beyond this point, CHO oxidation rises sharply (r = 0.99, $p < 0.001$), paralleling the gradual elevation in lactate levels. This pattern demonstrates a well-preserved metabolic flexibility, characterized by the ability to transition efficiently from predominant lipid oxidation to carbohydrate utilization as exercise intensity increases.

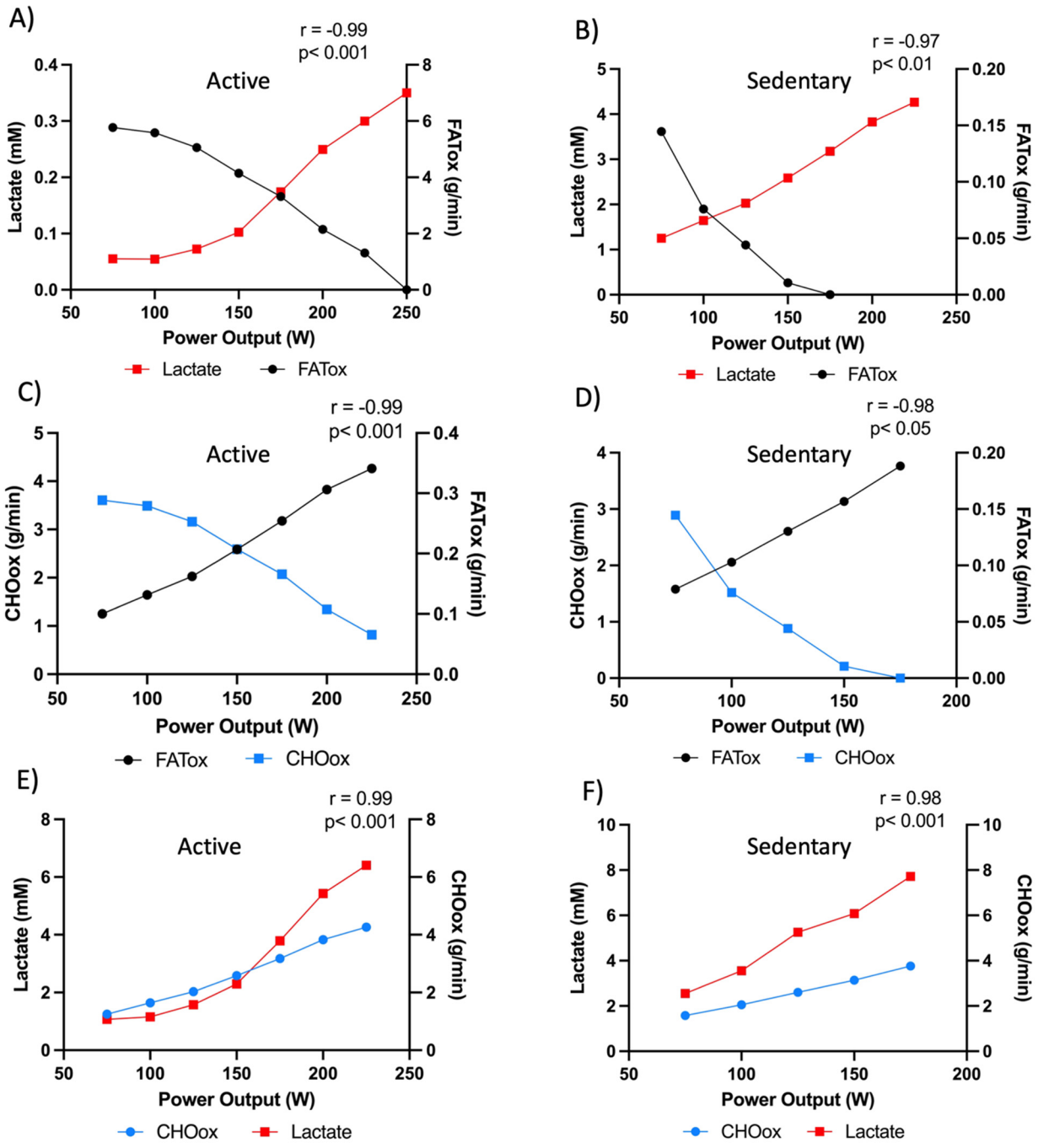

Figure 9. Substrate oxidation and lactate dynamics during incremental exercise in active and sedentary individuals. (**A**,**C**,**E**) Active individuals show progressive increases in fat oxidation (FATox) at low intensities, followed by a rise in carbohydrate oxidation (CHOOx) and lactate at higher workloads. (**B**,**D**,**F**) Sedentary individuals display lower FATox and earlier carbohydrate dependence, accompanied by a steep lactate rise even at moderate workloads. Correlation coefficients (r) reflect strong reciprocal relationships between FATox and lactate (**A**,**B**) and between CHOOx and FATox (**C**,**D**). These relationships illustrate preserved metabolic flexibility in active subjects and impaired substrate switching in sedentary counterparts, with lactate serving as a surrogate of mitochondrial oxidative efficiency.

Conversely, in sedentary individuals (Figure 9B,D,F), the metabolic profile is markedly altered. FATox remains substantially lower across all intensities, peaking near 0.15–0.2 g·min^{-1} and declining rapidly with rising power output, while lactate accumulates steeply from the earliest workloads ($r = -0.97$, $p < 0.01$). CHO oxidation dominates even

at low intensities, increasing linearly with power output, indicative of an early metabolic inflexibility. The elevated lactate concentrations at submaximal workloads suggest reduced mitochondrial pyruvate oxidation capacity and earlier increased glycolytic flux, consistent with impaired oxidative metabolism.

The strong reciprocal correlations between lactate and FATox ($r = -0.97$ to -0.99) across groups emphasize the tight coupling between lactate production and the suppression of fat oxidation. These findings position lactate not merely as a by-product of glycolysis but as a functional biomarker of substrate shift and mitochondrial efficiency. In metabolically flexible, active individuals, efficient pyruvate transport and oxidation within the mitochondria limit lactate accumulation and maintain high lipid utilization. In contrast, sedentary individuals exhibit an earlier glycolytic reliance and lactate accumulation consistent with reduced mitochondrial pyruvate oxidation capacity and lower overall oxidative phosphorylation.

Together, these results visualize metabolic flexibility as the dynamic intersection of fat and carbohydrate oxidation, with lactate serving as an integrated systemic marker of this shift. Active individuals maintain oxidative dominance over a wide intensity range, whereas sedentary individuals exhibit a constrained oxidative phenotype and early transition to glycolytic metabolism.

3.9. Rest–Exercise Correlations and Diagnostic Translation

Across participants, strong associations appeared between resting mitochondrial respiration and exercise-derived substrate oxidation. Resting fatty acid-supported oxygen flux, measured using palmitoylcarnitine and octanoylcarnitine, correlated robustly with in vivo fat oxidation rates during exercise ($r = 0.71$, $p < 0.001$), as shown in Figure 10. Similarly, total electron transfer system (ETS) capacity and ATP production at rest correlated with whole-body FATox during exercise ($r = 0.63$–0.70, $p < 0.01$), underscoring the translational link between cellular respiratory competence and systemic metabolic flexibility.

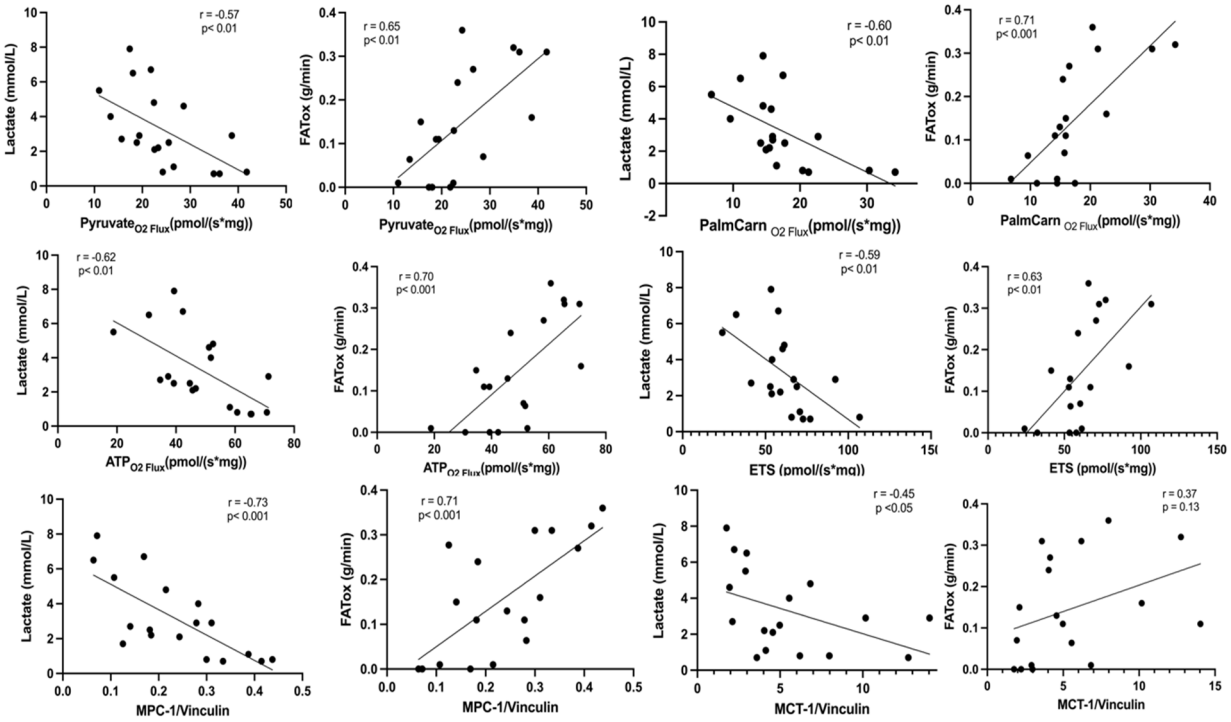

Figure 10. Correlations between resting mitochondrial respiration and exercise metabolic parameters. Scatterplots illustrate relationships between substrate-specific O_2 fluxes (pyruvate, palmitoylcarnitine, and octanoylcarnitine), electron transfer system capacity, and in vivo lactate and FATox responses.

Resting pyruvate-supported oxygen flux provided an additional layer of insight. Pyruvate oxidation correlated with in vivo FATox during exercise (r = 0.65, $p < 0.01$). Furthermore, MPC correlated with FATox during exercise (r = 0.71, $p < 0.001$), highlighting the central role of mitochondrial pyruvate handling in determining the transition between fat and carbohydrate utilization in vivo. Participants with higher pyruvate-supported flux at rest, reflecting greater MPC-dependent pyruvate transport, consistently showed lower lactate accumulation during exercise and a delayed shift toward carbohydrate reliance.

Maximal oxygen uptake (VO_2max) also correlated with ETS (r = 0.57, $p < 0.01$) and with combined ETS plus ATP synthase-linked capacity (r = 0.59, $p < 0.01$), indicating that higher electron transport and coupling efficiency at the muscle level manifest as superior aerobic performance.

Inverse correlations were observed between blood lactate concentrations during exercise and resting pyruvate-supported O_2 flux (r = −0.57, $p < 0.01$), palmitoylcarnitine oxidation (r = −0.60, $p < 0.01$), and MPC1 transporter (r = −0.73, $p < 0.001$). Lower mitochondrial oxidative capacity at rest, particularly reduced MPC-linked pyruvate flux, was associated with earlier lactate accumulation in vivo. This pattern is consistent with reduced mitochondrial pyruvate oxidation capacity shifting reliance toward glycolysis, elevating lactate production, and narrowing the metabolic flexibility window.

Together, these data provide an integrative framework linking cellular bioenergetics with systemic exercise physiology. They support the use of CPELT-derived measures such as FATox, and carbohydrate oxidation rates, crossover points, and lactate dynamics as noninvasive diagnostic tools to infer mitochondrial health and metabolic flexibility.

3.10. ^{13}C-Lactate Flux and Mitochondrial Coupling

During the initial phase of sample collection, a small number of tissue specimens were lost or yielded insufficient material for all assays due to handling limitations, resulting in slightly reduced sample sizes for certain correlations. Nevertheless, the relationships observed were strong and internally consistent, supporting their robustness.

Lactate flux, assessed through ^{13}C-lactate tracing, showed tight coupling with multiple indices of mitochondrial oxidative function (Figure 11). The flux of labeled lactate into mitochondrial respiration correlated positively with pyruvate-supported O_2 flux (r = 0.89, $p < 0.001$, d = 2.3) and MPC1 expression (r = 0.73, $p < 0.05$, d = 1.4), reinforcing the dependence of lactate oxidation on efficient pyruvate transport into the mitochondrial matrix. Similarly, lactate flux correlated with palmitoylcarnitine-supported respiration (r = 0.95, $p < 0.0001$, d = 3.1), octanoylcarnitine oxidation (r = 0.79, $p < 0.0001$, d = 1.7), ATP synthase-linked O_2 flux (r = 0.81, $p < 0.01$, d = 1.8), and total ETS capacity (r = 0.84, $p < 0.01$, d = 1.9). All associations demonstrated large effect sizes (d > 1.2), underscoring both their biological and statistical relevance and confirming that lactate oxidation is a fully integrated component of mitochondrial respiratory function.

An inverse association was observed between blood lactate concentration and lactate flux (r = −0.66, $p = 0.05$, d = 1.2), consistent with enhanced mitochondrial clearance capacity in individuals with higher oxidative function. No significant relationship was detected between total MCT1 expression and lactate flux (r = 0.35, $p = 0.13$, d = 0.6). This suggests that the regulation of lactate oxidation is governed primarily by mitochondrial MCT1 (not measured in the study), which facilitates intramitochondrial lactate transport and coupling to the MPC1–LDH complex, rather than by sarcolemmal MCT1 abundance measured in whole-muscle homogenates.

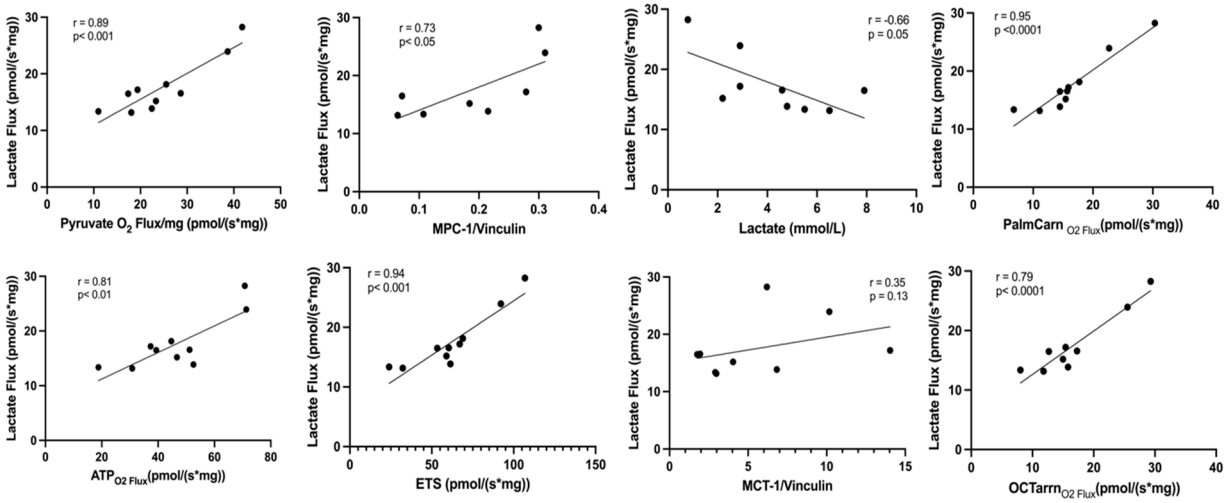

Figure 11. Correlations between ^{13}C-lactate flux and mitochondrial functional parameters. Scatterplots show associations between lactate-derived oxidative flux and pyruvate-supported O_2 flux, MPC1 expression, fatty-acid oxidation (palmitoylcarnitine and octanoylcarnitine), ATP-synthase-linked O_2 flux, and total electron transfer system (ETS) capacity. Strong positive correlations were observed across all parameters (r = 0.73–0.95, $p < 0.01$, Cohen's d = 1.4–3.1), indicating close coupling between lactate utilization and mitochondrial oxidative capacity. An inverse relationship was found between blood lactate concentration and lactate flux (r = −0.66, $p = 0.05$), whereas total MCT1 expression was not significantly related (r = 0.35, $p = 0.13$). Data suggest that mitochondrial, rather than sarcolemmal, MCT1 activity governs lactate oxidation within the mitochondria. Bars and regression lines represent mean ± SD; $p < 0.05$, $p < 0.01$.

Taken together, these findings indicate that higher mitochondrial lactate flux, representing the dynamic utilization of lactate-derived carbon, is strongly aligned with the key determinants of oxidative metabolism, including pyruvate oxidative capacity, fatty-acid oxidation, and ETS coupling. The magnitude of these associations supports the interpretation of lactate as both a metabolic substrate and a quantitative marker of mitochondrial efficiency.

4. Discussion

In this integrated cohort, sedentary individuals showed reduced mitochondrial respiratory capacity, lower MPC1 abundance with parallel reductions in pyruvate-stimulated respiration and [^{13}C]-labeling of TCA intermediates, lower CPT1 activity, lower total cardiolipin and L4CL content, and higher ROS production per unit O_2 flux, together with characteristic shifts in fat oxidation and lactate accumulation during CPELT (Figure 12). These findings extend, rather than overturn, established frameworks linking inactivity to reduced mitochondrial capacity and diminished metabolic flexibility by adding a converging set of observations focused on mitochondrial substrate-entry steps and by integrating cellular, metabolomic, isotope-tracing, and whole-body exercise measurements within a single cohort.

A novel aspect of this dataset is the demonstration of reduced MPC1 protein abundance in healthy sedentary muscle alongside preserved GLUT4, with parallel reductions in pyruvate-stimulated respiration and in [^{13}C]-lactate labeling of TCA intermediates. To our knowledge, MPC1 expression has not previously been reported across healthy sedentary versus active human skeletal muscle in this integrated way, and the differential pattern of preserved GLUT4 alongside reduced MPC1 is not readily explained by reductions in mitochondrial content alone (which would be expected to scale most mitochondrial proteins together). Whether this MPC1 difference is causally upstream of the broader mitochondrial

phenotype, or develops in parallel with it, cannot be resolved by the present cross-sectional design and will require longitudinal training/detraining and interventional studies.

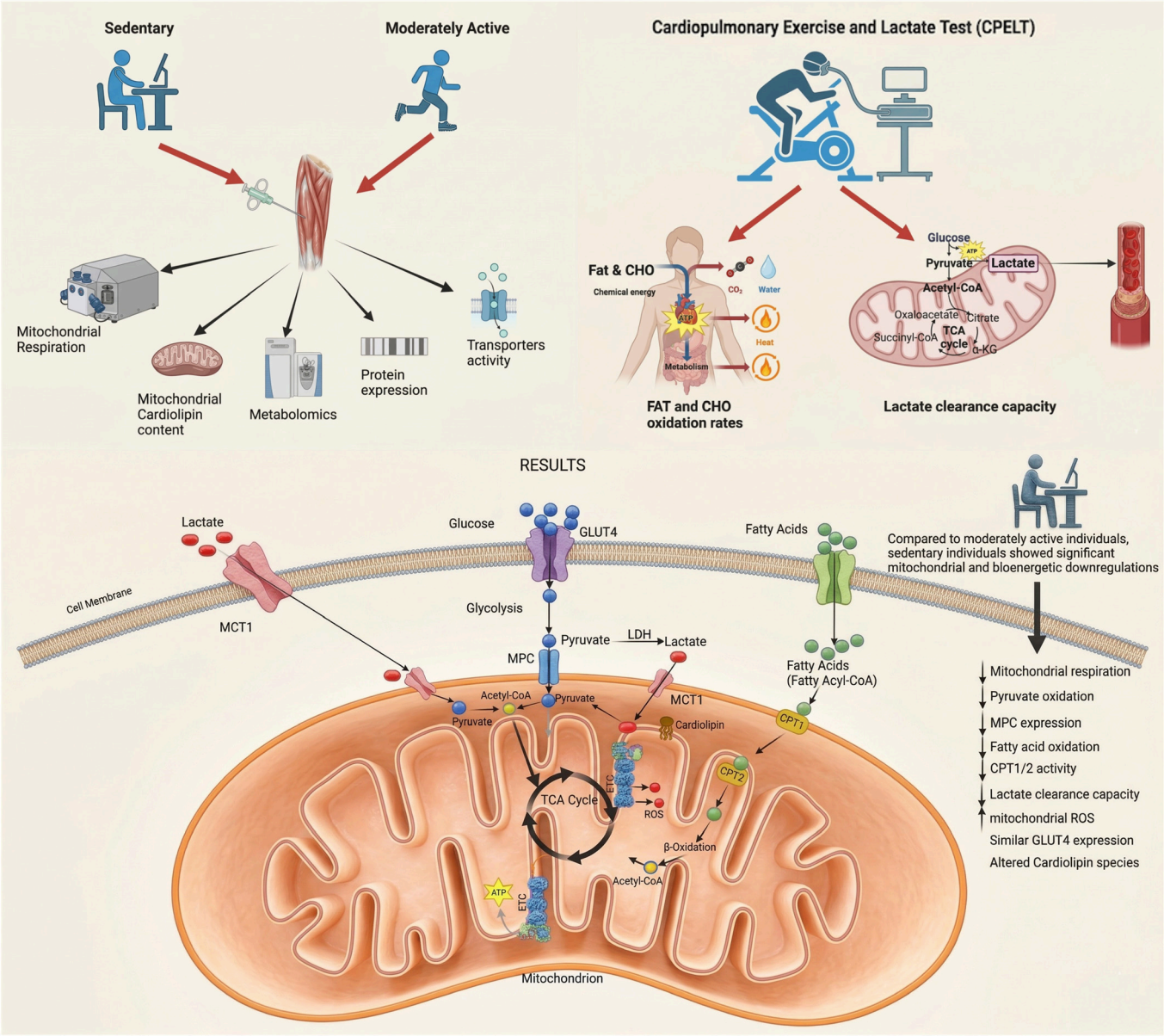

Figure 12. Schematic of skeletal muscle mitochondrion: SED side shows reduced MPC, CPT1, L4CL, and TCA flux with elevated ROS; AC side shows robust OXPHOS, fat oxidation, and lactate clearance. Arrows link to CPELT as a noninvasive diagnostic tool for mitochondrial health.

4.1. Mitochondrial Dysfunction and Substrate Oxidation

SED individuals showed substantial reductions across the electron transport system (Complex I, −36%; Complex II, −28%; ETS, −34%; and ATP synthase, −30%), indicating a broad depression of oxidative phosphorylation capacity and a reduced ability to sustain mitochondrial ATP production. This pattern aligns with classic and modern findings showing that physical inactivity decreases mitochondrial content, respiratory enzyme activity, and oxidative capacity in human skeletal muscle [22–25].

Such reductions limit the muscle's ability to oxidize both fatty acids and carbohydrates efficiently and place greater strain on upstream metabolic pathways. This weakened oxidative machinery is consistent with the reductions in substrate-stimulated respiration, TCA labeling, and exercise metabolic responses described later in the discussion. Together,

these observations suggest that inactivity is associated with a coordinated decline in mitochondrial structure and function that may contribute to the early development of metabolic inflexibility.

4.2. MPC1 as an Outstanding Differential Observation

Among all measured parameters, the most striking observation was the 49% reduction in mitochondrial pyruvate carrier 1 (MPC1) expression in SED individuals, alongside a 37% decline in pyruvate oxidation. Expression of GLUT4 transporters was similar in both groups. The differential expression of MPC1 in the absence of any difference in GLUT4 argues against adiposity as a confounding driver, since BMI-related metabolic impairment would be expected to affect sarcolemmal glucose transport capacity as well. Furthermore, all respirometry data were normalized to muscle wet weight, rendering whole-body body composition differences physiologically irrelevant to the mitochondrial comparisons reported here.

In our cohort, MPC1 abundance was 49% lower in SED muscle and tracked closely with reduced pyruvate-stimulated respiration and with reduced [^{13}C]-lactate labeling of citrate and malate, indicating lower mitochondrial pyruvate utilization in healthy sedentary muscle. Importantly, GLUT4 expression did not differ between groups, so glucose uptake at the sarcolemma was apparently preserved while downstream mitochondrial pyruvate handling was reduced. We interpret this not as evidence that MPC1 is the singular "primary" defect, nor as a wholesale displacement of sarcolemmal models, but as an additional, mitochondrially situated locus of impairment that complements established frameworks emphasizing mitochondrial content, oxidative-enzyme activity, lipid handling, and insulin signaling. The causal direction of these associations—whether reduced MPC1 is upstream of, parallel to, or downstream of the broader decline in mitochondrial capacity—cannot be established with the present cross-sectional design.

The convergent reductions across MPC1 protein abundance, pyruvate-stimulated respiration, [^{13}C]-lactate labeling of TCA intermediates, metabolomic profiles, and CPELT-derived lactate/FATox responses are mutually consistent and identify mitochondrial pyruvate handling as a candidate locus of early metabolic alteration in sedentary muscle. Whether reduced MPC1 abundance is upstream, parallel to, or downstream of broader changes in mitochondrial content and oxidative capacity cannot be resolved from the present cross-sectional design and will require longitudinal training/detraining studies with direct quantification of mitochondrial content.

Future studies incorporating direct mitochondrial-content quantification and normalization of MPC1 to structural mitochondrial markers such as VDAC or TOM20 will be required to address this question.

4.3. Integrative Metabolomics and MPC1 Limitation

Metabolomic profiles separated sedentary and active individuals. Active participants displayed lower glycolytic intermediates and a balanced spectrum of acylcarnitines, a pattern consistent with coordinated mitochondrial substrate use and adequate coupling between β-oxidation, TCA-cycle flux, and pyruvate oxidation. This represents a metabolically flexible phenotype in which fatty-acid and carbohydrate oxidation are efficiently matched to mitochondrial demand [29]. In contrast, sedentary individuals accumulated pyruvate-proximal glycolytic intermediates and glyceraldehyde-3-phosphate, along with lower levels of TCA intermediates and acylcarnitines. This pattern is consistent with reduced mitochondrial carbon entry and lower overall oxidative flux per unit tissue, features that align with the coordinated downscaling of mitochondrial substrate-handling capacity described above.

Stable isotope tracing with ^{13}C-lactate confirmed this interpretation. Sedentary individuals showed markedly reduced incorporation of ^{13}C into early TCA intermediates, including 40% lower citrate labeling and 35% lower malate labeling. This pattern matches classical MPC inhibition studies where diminished pyruvate entry results in lower labeling of TCA-cycle intermediates despite normal or elevated glycolytic flux [30].

Together, these metabolomic findings are consistent with the integrated tissue-level bioenergetic phenotype described throughout this manuscript, reflecting reduced oxidative substrate utilization and lower mitochondrial metabolic activity per unit muscle tissue in sedentary individuals.

4.4. Coordinated Downscaling of Mitochondrial Substrate-Handling Capacity

When considered together, the lower MPC1 abundance, lower CPT1 activity, reduced substrate-stimulated O_2 flux, lower cardiolipin content, reduced TCA labeling, and altered exercise lactate and FATox responses indicate a coordinated reduction in mitochondrial substrate-handling capacity per unit muscle tissue. These findings cannot establish that any individual component is intrinsically or selectively impaired beyond the overall reduction in mitochondrial abundance. Lower mitochondrial density per mg muscle may explain much of the observed phenotype by reducing the total mitochondrial membrane area, matrix volume, respiratory capacity, and enzyme and transporter pool available per unit tissue. MPC1 and CPT1 should therefore be interpreted as components of an integrated muscle-level bioenergetics phenotype.

Within this interpretation, however, MPC1 warrants specific attention as the outstanding differential observation in the dataset. MPC1 was reduced by 49% ($p = 0.005$, d = 2.1), the largest effect size in the study, while GLUT4, LDHA, and LDHB protein abundances were fully preserved. A pure reduction in mitochondrial content would be expected to scale mitochondrial membrane-bound proteins together while leaving cytosolic and sarcolemmal proteins unaffected; the selective magnitude of the MPC1 reduction relative to global ETS capacity (−34%) and relative to the preserved cytosolic proteins is consistent with this expectation but does not exclude the possibility of an additional disproportionate component. The reduced fractional [^{13}C]-lactate labeling of citrate (−40%) and malate (−35%) in fixed-mass tissue incubations similarly raises the question of whether pyruvate-entry capacity is disproportionately reduced, though this too cannot be resolved without direct mitochondrial-content normalization. These observations identify MPC1 and the pyruvate-entry step as a priority target for future studies incorporating citrate synthase activity, mtDNA copy number, TEM-based mitochondrial volume density, and normalization of mitochondrial proteins to structural mitochondrial markers such as VDAC, TOM20, or total OXPHOS complexes.

4.5. Comparative Role of Fatty-Acid Oxidation

In addition to pyruvate transport defect, reduced CPT1 activity and fatty-acid oxidation further compound the bioenergetic limitations of the sedentary phenotype. Impaired long-chain fatty-acid entry into mitochondria restricts β-oxidation and limits acetyl-CoA, reducing-equivalent (NADH and $FADH_2$) supply to the ETS. This dual restriction on carbohydrate and lipid catabolism narrows substrate flexibility and can lead to intramyocellular lipid accumulation, lipid spillover, and redox stress, which are well-established early features of metabolic inflexibility and insulin resistance [31–34].

4.6. Cardiolipin Remodeling and Cristae Function

Beyond its structural role, the decline in L4-cardiolipin observed in sedentary muscle may destabilize several functionally coupled components of the inner mitochondrial membrane. L4CL is required for the stability of respiratory supercomplexes and for the efficient

transfer of electrons from Complex I through Complexes III and IV. Loss or oxidation of L4CL weakens these interactions and decreases the efficiency of electron flow, which promotes ROS generation [35,36]. Higher monolysocardiolipin (MLCL) in AC suggests more active CL remodeling, supporting mitochondrial maintenance under regular physical activity [37]. Together, these mechanistic insights provide a biologically coherent explanation for how the decline in L4CL in sedentary muscle could contribute to the reduced pyruvate oxidation and electron transport capacity observed in our dataset.

4.7. ROS Production and Redox Balance

Sedentary individuals showed a higher ROS/O_2 flux ratio than active individuals, indicating greater net ROS efflux per unit of respiratory throughput. This system-level observation is descriptive and does not allow for unambiguous mechanistic interpretation. Two plausible explanations exist. First, lower mitochondrial respiratory flux and elevated membrane potential in sedentary muscle could increase the probability of incomplete electron transfer and superoxide formation at the respiratory chain, consistent with prior observations [38,39]. Second, exercise training is known to upregulate mitochondrial antioxidant networks, including MnSOD and GPx; active individuals may therefore show a lower net ROS/O_2 ratio because greater intra-mitochondrial antioxidant buffering capacity neutralizes superoxide before it escapes the fiber, rather than because their respiratory chains produce intrinsically less ROS per unit flux. The present data cannot distinguish between these interpretations.

Active participants produced higher absolute ROS, consistent with their greater respiratory flux. These differences in net ROS efflux between groups are retained as a component of the descriptive tissue-level bioenergetic phenotype. Whether they reflect altered respiratory-chain electron leak, differences in intra-mitochondrial antioxidant capacity, or both is an open question that future studies conducting direct measurement of mitochondrial antioxidant enzyme activity (MnSOD, GPx, and catalase) should address [40–42].

4.8. Exercise Correlations and Translational Value

In active individuals, lactate and FATox displayed near-perfect inverse coupling ($r = -0.99$, $p < 0.001$; Figure 9A), reflecting efficient mitochondrial function, substrate regulation, and overall metabolic flexibility. As we previously showed [21], this pattern indicates preserved coordination between carbohydrate and lipid oxidation during incremental workloads. By contrast, sedentary individuals exhibited an early lactate inflection and a sharp decline in FATox even at mild workloads (~100 W; Figure 9B), denoting metabolic inflexibility and impaired mitochondrial substrate reprograming.

This phenomenon is mechanistically consistent with the inhibitory role of lactate on lipid metabolism. Elevated blood lactate levels have been shown to suppress adipose lipolysis [43], while our recent findings demonstrate that intracellular lactate also reduces CPT1 and CPT2 activity [44], directly limiting mitochondrial fatty-acid entry and oxidation. Thus, lactate functions not only as a redox intermediate but also as an endocrine and autocrine regulator that constrains fat oxidation when chronically elevated.

CHOox and lactate increased in parallel in both groups ($r \approx 0.99$, $p < 0.001$; Figure 9E,F). However, in sedentary participants, the crossover point between FATox and CHOox occurred at significantly lower workloads, quantitatively demonstrating reduced mitochondrial flexibility and a premature transition toward carbohydrate dependence (Figure 9C,D). These results indicate that the balance between lactate accumulation and FATox during graded CPELT provides a direct, mechanistically interpretable index of mitochondrial substrate-oxidative capacity.

4.9. Linking Exercise Metabolism to Mitochondrial Function

When exercise-derived variables were cross-correlated with resting mitochondrial parameters (Figures 11 and 12), consistent multi-scale relationships emerged, linking cellular and whole-body bioenergetics. Exercise blood lactate at moderate intensities correlated inversely with key mitochondrial markers, including pyruvate oxidation ($r = -0.57$, $p < 0.01$), palmitoylcarnitine-supported FA oxidation ($r = -0.60$, $p < 0.01$), ETS capacity ($r = -0.59$, $p < 0.01$), ATP-synthase-coupled flux ($r = -0.62$, $p < 0.01$), and MPC1 expression ($r = -0.73$, $p < 0.01$). Exercise FATox from CPELT, conversely, correlated positively with the same mitochondrial features: pyruvate oxidation ($r = 0.65$, $p < 0.01$), palmitoylcarnitine flux ($r = 0.71$, $p < 0.001$), ETS capacity ($r = 0.63$, $p < 0.01$), ATP-synthase flux ($r = 0.70$, $p < 0.001$), and MPC1 expression ($r = 0.71$, $p < 0.001$).

Sarcolemmal MCT1 expression displayed weaker associations ($r = 0.37$), indicating that intracellular oxidative capacity, rather than transmembrane transport, determines exercise metabolic responses in sedentary individuals.

Recent evidence indicates that a distinct pool of MCT1 resides on the inner mitochondrial membrane, functionally associated with LDH and MPC1 as part of the mitochondrial lactate oxidation complex (mLOC) [45,46]. The dissociation between total MCT1 protein expression and lactate oxidation rates supports the hypothesis that the limitation is not sarcolemmal uptake, but rather intramitochondrial transport and oxidation, likely involving the mLOC, which was not directly quantified here. mLOC coupling to MPC1 as part of a mitochondrial reticulum [46], provides a structural basis for the tight correlation observed between lactate flux, pyruvate oxidation, and ETS capacity in the present study.

Furthermore, lactate flux, representing the dynamic mitochondrial utilization of lactate, further reinforced this link between rest and exercise physiology (Figure 11). Lactate flux correlated strongly and positively with pyruvate oxidation ($r = 0.89$, $p < 0.001$), MPC1 expression ($r = 0.73$, $p < 0.05$), palmitoylcarnitine-driven FA oxidation ($r = 0.95$, $p < 0.0001$), octanoylcarnitine oxidation ($r = 0.79$, $p < 0.0001$), ETS capacity ($r = 0.84$, $p < 0.01$), and ATP-synthase-coupled respiration ($r = 0.81$, $p < 0.01$). It correlated inversely with circulating blood lactate ($r = -0.66$, $p = 0.05$) and showed only a modest relationship with MCT1 expression ($r = 0.35$, $p = 0.13$ ns), suggesting that mitochondrial oxidative capacity, rather than sarcolemmal transport, is the primary determinant of lactate clearance in this cohort.

Figure 10 reveals that exercise blood lactate and FATox are complementary, mechanistically grounded surrogates of mitochondrial dysfunction. Together, they integrate substrate entry, TCA flux, and electron transport into two clinically measurable outputs: ΔLactate, which reflects pyruvate transport and carbohydrate oxidation efficiency, and ΔFATox, which reflects long-chain fatty-acid transport and β-oxidation capacity.

4.10. Translational Clinical Implications

The combined alterations in lactate handling and fatty-acid oxidation have direct clinical value. For example, a simple observation such as blood lactate above 2.5 mmol/L together with FATox below 0.4 g per min during moderate exercise at 50 to 60 percent of VO_2max can serve as an early physiological signature of subclinical mitochondrial dysfunction. These values reflect impaired pyruvate oxidation and reduced long-chain fatty-acid utilization, two defects that commonly appear long before overt metabolic disease develops.

The integration of these variables into a single submaximal cardiopulmonary exercise test provides a practical and scalable mitochondrial health index. This ΔLactate + ΔFATox dyad captures the two major arms of substrate oxidation. Together, these variables define a noninvasive physiological signature of mitochondrial function, directly linking systemic exercise responses to underlying cellular bioenergetics. ΔLactate reflects the efficiency of

glucose metabolism and the capacity of pyruvate to enter mitochondria and be oxidized through the electron transport system. ΔFATox monitors the lipid oxidative pathways linked to CPT1 function and β-oxidation. Together, they allow clinicians and researchers to identify whether the primary metabolic limitation is related to carbohydrate oxidation, lipid oxidation, or both, arising from early mitochondrial decay or dysfunction.

This approach has the advantage of being noninvasive, repeatable, and sensitive to early mitochondrial impairment. It also maps directly onto therapeutic interventions, mainly through exercise. Improvements in ΔLactate + ΔFATox suggest successful restoration of substrate oxidation through an overall improvement in pyruvate and fatty-acid transport and mitochondrial function. Future research should expand to include women, explore epigenetic regulation of MPC (histone lactylation and miRNA suppression), and evaluate exercise or MPC-activating interventions as reversible therapies for early mitochondrial dysfunction.

In summary, lactate and FATox responses obtained from a simple submaximal exercise test offer complementary and mechanistically grounded insight into mitochondrial efficiency. Embedding these variables into routine CPELT would allow clinicians to adopt a clinically meaningful diagnostic tool for early detection of metabolic risk, personalized intervention, and long-term monitoring of mitochondrial and metabolic health.

4.11. Evolutionary and Clinical Perspective

Sedentarism is not a neutral human condition but a recent biological insult. From an evolutionary standpoint, mitochondria originated as energy-producing symbionts selected under near-constant physical demand. When this demand disappears, mitochondrial structure and function undergo molecular atrophy. Our findings frame sedentarism as an early, reversible metabolic injury rather than an inevitable outcome of modern life. The convergence of molecular, metabolic, and physiological evidence presented here indicates that loss of mitochondrial function is one of the first measurable steps in the trajectory toward non-communicable disease.

The bioenergetic plasticity observed here between sedentary and active human skeletal muscle reflects a broader and evolutionarily conserved mammalian strategy of matching mitochondrial capacity to local energetic demand. Comparative physiological work across mammalian tissues has shown that OXPHOS capacity and respiratory enzyme activities are finely tailored to the differing energetic requirements of distinct organs and fiber types, with corresponding tissue-specific patterns of mitochondrial activity, biogenesis, and mitochondrial protein gene expression [47]. This metabolic scaling depends in large part on the targeted regulation of nuclear-encoded mitochondrial protein genes, particularly those that assemble OXPHOS Complex I, which adjust cellular energy production dynamically to match high-demand tissues [48]. The coordinated reduction in both pyruvate entry through MPC1 and long-chain fatty-acid entry through CPT1 identified in our sedentary cohort parallels the coordinated regulation of nuclear-encoded mitochondrial genes governing lipid and carbohydrate metabolism that has been described across mammalian tissues with differing metabolic demands [49]. Viewed through this comparative lens, the human sedentary phenotype is consistent with a downregulation, within an evolutionarily conserved bioenergetic network, of the mitochondrial substrate-entry and oxidative machinery that is normally tuned to sustained physical demand. We emphasize, in line with the moderated framing used throughout the revised manuscript, that this comparative interpretation is offered as context rather than as evidence of causation, which remains to be established by longitudinal and interventional human studies.

4.12. Limitations and Future Directions

This study has some limitations. The sample size was modest, although it is comparable to other mechanistic human studies involving biopsies, metabolomics, and high-resolution respirometry, and the data were supported by a priori power analysis. Furthermore, the large effect sizes observed across key mitochondrial variables (Cohen's $d > 1.2$) underscore the biological magnitude of these differences. However, the cohort included only men, so the findings may not generalize to women. Sex-related differences in skeletal-muscle metabolism and sex-hormone effects on mitochondrial function and lipid oxidation are well documented, and the MPC1, CPT1, and cardiolipin signatures observed here may differ quantitatively in women across the menstrual cycle and menopausal status; inclusion of female cohorts is therefore an important next step. Sedentary participants had slightly higher BMI, which may contribute to some of the metabolic differences. Direct quantification of mitochondrial content (e.g., citrate synthase activity, mtDNA copy number, or transmission electron microscopy) was not performed in this cohort; all functional and biochemical measurements are reported per mg of muscle wet tissue, which is the standard physiological unit for muscle considered a metabolic organ and the unit in which content surrogates themselves are typically expressed. Future studies that pair direct content quantification with the functional readouts used here would further apportion the relative contributions of mitochondrial abundance and per-mitochondrion function, although several features of the present dataset (notably the selective reduction of MPC1 with preserved GLUT4, LDHA, and LDHB, and the reduced fractional [^{13}C]-labeling of TCA intermediates from lactate) are not parsimoniously explained by content effects alone. Finally, this was a cross-sectional comparison. Longitudinal detraining/retraining studies will be necessary to map the temporal sequence of changes in mitochondrial content, MPC1 abundance, substrate handling, and metabolic flexibility.

4.13. Future Directions

Future work should include women and larger, ethnically diverse cohorts. Interventional studies with structured training will help determine whether the MPC1 and CPT1 signatures are reversible and whether they improve in parallel with mitochondrial function and substrate utilization. Longitudinal designs will be important to test whether this phenotype precedes, parallels, or follows changes in insulin sensitivity. Stable isotope flux methods can be expanded to quantify tissue-specific lactate oxidation and its regulation by MPC1 and redox state. Because sedentary behavior exists on a continuum rather than as a binary category, future cohorts should objectively quantify habitual physical activity and non-exercise activity thermogenesis (NEAT) using validated tri-axial accelerometry (e.g., wrist- or thigh-worn devices over $\geq$7 days, with concurrent inclinometry to discriminate sitting from light ambulation). Such objective phenotyping would allow the sedentary-to-active continuum to be modeled quantitatively against the mitochondrial and CPELT endpoints described here and would strengthen the precision of inclusion criteria in subsequent longitudinal and interventional trials. In addition, given the dissociation observed in our data between whole-muscle MCT1 expression and mitochondrial lactate oxidation, future studies should isolate mitochondrial fractions (e.g., differential centrifugation followed by Percoll-gradient purification, with VDAC or TOMM20 used as outer-membrane markers) and directly quantify inner-mitochondrial MCT1 protein abundance and its association with MPC1 and LDH within the proposed mitochondrial lactate oxidation complex (mLOC). Pairing such mitochondrial-fraction immunoblotting with super-resolution or proximity-ligation imaging would directly test the structural prediction that intramitochondrial lactate transport, rather than sarcolemmal MCT1 abundance, is the principal determinant of lactate oxidation in skeletal muscle. Finally, external validation

of physiological markers from submaximal CPELT could allow for the development of a clinical tool for early mitochondrial health assessment.

5. Conclusions

These findings support the presence of an integrated sedentary skeletal-muscle bioenergetic phenotype characterized by lower tissue-level mitochondrial oxidative capacity, reduced substrate-handling markers, altered cardiolipin abundance, and diminished metabolic flexibility. Within this phenotype, the 49% reduction in MPC1 alongside preserved GLUT4, LDHA, and LDHB represents a differential observation of the dataset, raising the hypothesis that mitochondrial pyruvate-entry capacity may be disproportionately reduced relative to overall mitochondrial abundance. Future studies incorporating direct mitochondrial-content measurements and mitochondrial-protein normalization will be required to test this hypothesis and to determine whether MPC1, CPT1, or related transport systems are altered disproportionately to mitochondrial biomass.

Supplementary Materials: The following supporting information can be downloaded at: https://www.mdpi.com/article/10.3390/clinbioenerg2030010/s1. Figure S1. Representative Jess capillary electropherogram illustrating MPC1 (~12 kDa) and vinculin loading control (~116 kDa) protein expression across the full cohort. Lanes 2–10 correspond to sedentary (SED) individuals and lanes 11–21 to active (AC) individuals (1.1 µg/µL total protein per lane; lane 1, biotinylated molecular weight ladder). The red box highlights the active subject group, in which MPC1 band intensity is visibly greater relative to sedentary individuals. Vinculin (~116 kDa) served as the total protein loading control. All samples were run at 1.1 µg/µL using the Jess automated capillary Western system (ProteinSimple, San Jose, CA, USA) and Compass for Simple Western software (version 6.1.0). MPC1 antibody: Abcam, ab176559, Cambridge, UK.

Author Contributions: I.S.-M. conceptualization, supervision, exercise testing, data analysis, manuscript writing, and funding acquisition; J.L.M., exercise testing and data analysis; G.C.S., cardiolipin analysis; A.D., D.S., and T.N., metabolomics and fluxomics; J.H., muscle biopsies. All authors have read and agreed to the published version of the manuscript.

Funding: A gift fund-34, D-0034889, provided the funds for this study.

Institutional Review Board Statement: The study was conducted in accordance with the Declaration of Helsinki and approved by the Colorado Multiple Institutional Review Board (protocol code 17-1095; approval date, 6 November 2018).

Informed Consent Statement: Informed consent was obtained from all subjects involved in the study.

Data Availability Statement: Raw data (metabolomics, respirometry, and exercise) will be available upon publication. Contact the corresponding author for interim access.

Acknowledgments: We thank the University of Colorado Anschutz Medical Campus for facilities, technical staff, and participants.

Conflicts of Interest: The authors declare no conflicts of interest.

References

1. Ahmed, H.M.; Blaha, M.J.; Nasir, K.; Rivera, J.J.; Blumenthal, R.S. Effects of physical activity on cardiovascular disease. *Am. J. Cardiol.* **2012**, *109*, 288–295. [CrossRef] [PubMed]
2. Berlin, J.A.; Colditz, G.A. A meta-analysis of physical activity in the prevention of coronary heart disease. *Am. J. Epidemiol.* **1990**, *132*, 612–628. [CrossRef] [PubMed]
3. Chen, H.; Zhang, S.; Schwarzschild, M.; Hernan, M.; Ascherio, A. Physical activity and the risk of Parkinson disease. *Neurology* **2005**, *64*, 664–669. [CrossRef] [PubMed]

4. Colberg, S.R.; Sigal, R.J.; Yardley, J.E.; Riddell, M.C.; Dunstan, D.W.; Dempsey, P.C.; Horton, E.S.; Castorino, K.; Tate, D.F. Physical activity/exercise and diabetes: A position statement of the American Diabetes Association. *Diabetes Care* **2016**, *39*, 2065–2079. [CrossRef] [PubMed]
5. Durstine, J.L.; Gordon, B.; Wang, Z.; Luo, X. Chronic disease and the link to physical activity. *J. Sport. Health Sci.* **2013**, *2*, 3–11. [CrossRef]
6. Friedenreich, C.M.; Ryder-Burbidge, C.; McNeil, J. Physical activity, obesity and sedentary behavior in cancer etiology: Epidemiologic evidence and biologic mechanisms. *Mol. Oncol.* **2021**, *15*, 790–800. [PubMed]
7. Grill, S.; Yahiaoui-Doktor, M.; Dukatz, R.; Lammert, J.; Ullrich, M.; Engel, C.; Pfeifer, K.; Basrai, M.; Siniatchkin, M.; Schmidt, T.; et al. Smoking and physical inactivity increase cancer prevalence in BRCA-1 and BRCA-2 mutation carriers. *Arch. Gynecol. Obstet.* **2017**, *296*, 1135–1144. [CrossRef] [PubMed]
8. Kohl, H.W. Physical activity and cardiovascular disease: Evidence for a dose response. *Med. Sci. Sports Exerc.* **2001**, *33*, S472–S483. [CrossRef] [PubMed]
9. LaMonte, M.J.; Blair, S.N.; Church, T.S. Physical activity and diabetes prevention. *J. Appl. Physiol.* **2005**, *99*, 1205–1213. [CrossRef] [PubMed]
10. Mctiernan, A.; Friedenreich, C.M.; Katzmarzyk, P.T.; Powell, K.E.; Macko, R.; Buchner, D.; Pescatello, L.S.; Bloodgood, B.; Tennant, B.; Vaux-Bjerke, A.; et al. Physical activity in cancer prevention and survival: A systematic review. *Med. Sci. Sports Exerc.* **2019**, *51*, 1252. [CrossRef] [PubMed]
11. Powell, K.E.; Thompson, P.D.; Caspersen, C.J.; Kendrick, J.S. Physical activity and the incidence of coronary heart disease. *Annu. Rev. Public. Health* **1987**, *8*, 253–287. [CrossRef] [PubMed]
12. Rolland, Y.; van Kan, G.A.; Vellas, B. Physical activity and Alzheimer's disease: From prevention to therapeutic perspectives. *J. Am. Med. Dir. Assoc.* **2008**, *9*, 390–405. [CrossRef] [PubMed]
13. Santos-Lozano, A.; Pareja-Galeano, H.; Sanchis-Gomar, F.; Quindós-Rubial, M.; Fiuza-Luces, C.; Cristi-Montero, C.; Emanuele, E.; Garatachea, N.; Lucia, A. Physical activity and Alzheimer disease: A protective association. *Mayo Clin. Proc.* **2016**, *91*, 999–1020. [CrossRef] [PubMed]
14. Stephen, R.; Hongisto, K.; Solomon, A.; Lönnroos, E. Physical activity and Alzheimer's disease: A systematic review. *J. Gerontol. A Biol. Sci. Med. Sci.* **2017**, *72*, 733–739. [CrossRef] [PubMed]
15. Blair, S.N. Physical inactivity: The biggest public health problem of the 21st century. *Br. J. Sports Med.* **2009**, *43*, 1–2. [PubMed]
16. World Health Organization. *Global Status Report on Physical Activity 2022*; World Health Organization: Geneva, Switzerland, 2022.
17. San-Millán, I. The Key Role of Mitochondrial Function in Health and Disease. *Antioxidants* **2023**, *12*, 782. [CrossRef] [PubMed]
18. DeFronzo, R.A.; Tripathy, D. Skeletal muscle insulin resistance is the primary defect in type 2 diabetes. *Diabetes Care* **2009**, *32*, S157–S163. [CrossRef] [PubMed]
19. Bricker, D.K.; Taylor, E.B.; Schell, J.C.; Orsak, T.; Boutron, A.; Chen, Y.-C.; Cox, J.E.; Cardon, C.M.; Van Vranken, J.G.; Dephoure, N.; et al. A mitochondrial pyruvate carrier required for pyruvate uptake in yeast, Drosophila, and humans. *Science* **2012**, *337*, 96–100. [CrossRef] [PubMed]
20. Herzig, S.; Raemy, E.; Montessuit, S.; Veuthey, J.-L.; Zamboni, N.; Westermann, B.; Kunji, E.R.S.; Martinou, J.-C. Identification and functional expression of the mitochondrial pyruvate carrier. *Science* **2012**, *337*, 93–96. [CrossRef] [PubMed]
21. San-Millan, I.; Brooks, G.A. Assessment of Metabolic Flexibility by Means of Measuring Blood Lactate, Fat, and Carbohydrate Oxidation Responses to Exercise in Professional Endurance Athletes and Less-Fit Individuals. *Sports Med.* **2018**, *48*, 467–479. [CrossRef] [PubMed]
22. Coyle, E.F.; Martin, W.H.; Bloomfield, S.A.; Lowry, O.H.; Holloszy, J.O. Effects of detraining on responses to submaximal exercise. *J. Appl. Physiol.* **1985**, *59*, 853–859. [CrossRef] [PubMed]
23. Fritzen, A.M.; Thøgersen, F.B.; Thybo, K.; Vissing, C.R.; Krag, T.O.; Ruiz-Ruiz, C.; Risom, L.; Wibrand, F.; Høeg, L.D.; Kiens, B.; et al. Adaptations in Mitochondrial Enzymatic Activity Occurs Independent of Genomic Dosage in Response to Aerobic Exercise Training and Deconditioning in Human Skeletal Muscle. *Cells* **2019**, *8*, 237. [CrossRef] [PubMed]
24. Houmard, J.A.; Hortobágyi, T.; Johns, R.A.; Bruno, N.J.; Nute, C.C.; Shinebarger, M.H.; Welborn, J.W. Effect of short-term training cessation on performance measures in distance runners. *Int. J. Sports Med.* **1992**, *13*, 572–576. [CrossRef] [PubMed]
25. Houston, M.E.; Bentzen, H.; Larsen, H. Interrelationships between skeletal muscle adaptations and performance as studied by detraining and retraining. *Acta Physiol. Scand.* **1979**, *105*, 163–170. [CrossRef] [PubMed]
26. Gnaiger, E.; Kuznetsov, A.V.; Schneeberger, S.; Seiler, R.; Brandacher, G.; Steurer, W.; Margreiter, R. Mitochondria in the cold. In *Life in the Cold: Eleventh International Hibernation Symposium*; Springer: Berlin/Heidelberg, Germany, 2000.
27. Sparagna, G.C.; Johnson, C.A.; McCune, S.A.; Moore, R.L.; Murphy, R.C. Quantitation of cardiolipin molecular species in spontaneously hypertensive heart failure rats using electrospray ionization mass spectrometry. *J. Lipid Res.* **2005**, *46*, 1196–1204. [CrossRef] [PubMed]
28. Frayn, K.N. Calculation of substrate oxidation rates in vivo from gaseous exchange. *J. Appl. Physiol.* **1983**, *55*, 628–634. [CrossRef] [PubMed]

29. Muoio, D.M. Metabolic inflexibility: When mitochondrial indecision leads to metabolic gridlock. *Cell* **2014**, *159*, 1253–1262. [CrossRef] [PubMed]
30. Vacanti, N.M.; Divakaruni, A.S.; Green, C.R.; Parker, S.J.; Henry, R.R.; Ciaraldi, T.P.; Murphy, A.N.; Metallo, C.M. Regulation of substrate utilization by the mitochondrial pyruvate carrier. *Mol. Cell* **2014**, *56*, 425–435. [CrossRef] [PubMed]
31. Amati, F.; Dubé, J.J.; Alvarez-Carnero, E.; Edreira, M.M.; Chomentowski, P.; Coen, P.M.; Switzer, G.E.; Bickel, P.E.; Stefanovic-Racic, M.; Toledo, F.G.; et al. Skeletal Muscle Triglycerides, Diacylglycerols, and Ceramides in Insulin Resistance. *Diabetes* **2011**, *60*, 2588–2597. [CrossRef] [PubMed]
32. Bergman, B.C.; Goodpaster, B.H. Exercise and Muscle Lipid Content, Composition, and Localization: Influence on Muscle Insulin Sensitivity. *Diabetes* **2020**, *69*, 848–858. [CrossRef] [PubMed]
33. Bergman, B.C.; Perreault, L.; Hunerdosse, D.M.; Koehler, M.C.; Samek, A.M.; Eckel, R.H. Increased intramuscular lipid synthesis and low saturation relate to insulin sensitivity in endurance-trained athletes. *J. Appl. Physiol.* **2010**, *108*, 1134–1141. [CrossRef] [PubMed]
34. Goodpaster, B.H.; He, J.; Watkins, S.; Kelley, D.E. Skeletal Muscle Lipid Content and Insulin Resistance: Evidence for a Paradox in Endurance-Trained Athletes. *J. Clin. Endocrinol. Metab.* **2001**, *86*, 5755–5761. [CrossRef] [PubMed]
35. Paradies, G.; Paradies, V.; De Benedictis, V.; Ruggiero, F.M.; Petrosillo, G. Functional role of cardiolipin in mitochondrial bioenergetics. *Biochim. Biophys. Acta* **2014**, *1837*, 408–417. [CrossRef] [PubMed]
36. Pfeiffer, K.; Gohil, V.; Stuart, R.A.; Hunte, C.; Brandt, U.; Greenberg, M.L.; Schägger, H. Cardiolipin stabilizes respiratory chain supercomplexes. *J. Biol. Chem.* **2003**, *278*, 52873–52880. [CrossRef] [PubMed]
37. Chicco, A.J.; Sparagna, G.C. Role of cardiolipin alterations in mitochondrial dysfunction and disease. *Am. J. Physiol. Cell Physiol.* **2007**, *292*, C33–C44. [CrossRef] [PubMed]
38. Brand, M.D. The sites and topology of mitochondrial superoxide production. *Exp. Gerontol.* **2010**, *45*, 466–472. [CrossRef] [PubMed]
39. Murphy, M.P. How mitochondria produce reactive oxygen species. *Biochem. J.* **2009**, *417*, 1–13. [PubMed]
40. Gomez-Cabrera, M.-C.; Domenech, E.; Romagnoli, M.; Arduini, A.; Borras, C.; Pallardo, F.V.; Sastre, J.; Viña, J. Oral administration of vitamin C decreases muscle mitochondrial biogenesis and hampers training-induced adaptations in endurance performance. *Am. J. Clin. Nutr.* **2008**, *87*, 142–149. [CrossRef] [PubMed]
41. Hood, D.A.; Uguccioni, G.; Vainshtein, A.; D'Souza, D. Mechanisms of exercise-induced mitochondrial biogenesis in skeletal muscle: Implications for health and disease. *Compr. Physiol.* **2011**, *1*, 1119–1134. [CrossRef] [PubMed]
42. Ristow, M.; Zarse, K.; Oberbach, A.; Klöting, N.; Birringer, M.; Kiehntopf, M.; Stumvoll, M.; Kahn, C.R.; Blüher, M. Antioxidants prevent health-promoting effects of physical exercise in humans. *Proc. Natl. Acad. Sci. USA* **2009**, *106*, 8665–8670. [CrossRef] [PubMed]
43. Liu, C.; Wu, J.; Zhu, J.; Kuei, C.; Yu, J.; Shelton, J.; Sutton, S.W.; Li, X.; Yun, S.J.; Mirzadegan, T.; et al. Lactate inhibits lipolysis in fat cells through activation of an orphan G-protein-coupled receptor, GPR81. *J. Biol. Chem.* **2009**, *284*, 2811–2822. [CrossRef] [PubMed]
44. San-Millan, I.; Sparagna, G.C.; Chapman, H.L.; Warkins, V.L.; Chatfield, K.C.; Shuff, S.R.; Martinez, J.L.; Brooks, G.A. Chronic Lactate Exposure Decreases Mitochondrial Function by Inhibition of Fatty Acid Uptake and Cardiolipin Alterations in Neonatal Rat Cardiomyocytes. *Front. Nutr.* **2022**, *9*, 809485. [CrossRef] [PubMed]
45. Hashimoto, T.; Hussien, R.; Brooks, G.A. Colocalization of MCT1, CD147, and LDH in mitochondrial inner membrane of L6 muscle cells: Evidence of a mitochondrial lactate oxidation complex. *Am. J. Physiol. Endocrinol. Metab.* **2006**, *290*, E1237–E1244. [CrossRef] [PubMed]
46. Leija, R.G.; Vazquez-Medina, J.P.; Brooks, G.A. Resilience of the mitochondrial reticulum in aging. *Am. J. Physiol. Endocrinol. Metab.* **2025**, *329*, E477–E494. [CrossRef] [PubMed]
47. Sadeesh, E.M.; Singla, N.; Lahamge, M.S.; Kumari, S.; Ampadi, A.N.; Anuj, M. Tissue heterogeneity of mitochondrial activity, biogenesis and mitochondrial protein gene expression in buffalo. *Mol. Biol. Rep.* **2023**, *50*, 5255–5266. [CrossRef] [PubMed]
48. Sadeesh, E.M.; Lahamge, M.S.; Malik, A.; Ampadi, A.N. Nuclear genome-encoded mitochondrial OXPHOS Complex I genes in female buffalo show tissue-specific differences. *Mol. Biotechnol.* **2025**, *67*, 2411–2427. [CrossRef] [PubMed]
49. Sadeesh, E.M.; Lahamge, M.S.; Kumari, S.; Singh, P. Tissue-specific diversity of nuclear-encoded mitochondrial genes related to lipid and carbohydrate metabolism in buffalo. *Mol. Biotechnol.* **2026**, *68*, 335–350. [CrossRef] [PubMed]